Process-Structure Linkages in Materials via Deep Learning from Phase-Field Simulation Data

A Thesis

Presented in Partial Fulfillment of the Requirements for the

Degree of Master of Engineering

with a

Major in Materials Science & Engineering

in the

College of Graduate Studies

University of Idaho

by

Isaac I. Curtis

Major Professor: Samrat Choudhury, Ph.D.

Committee Members: Indrajit Charit, Ph.D.; Mark Roll, Ph.D.; Vishnu Boddeti, Ph.D.

Department Administrator: Erik Aston, Ph.D.

May 2019

Authorization to Submit Thesis

This thesis of Isaac I. Curtis, submitted for the degree of Master of Engineering with a Major in Materials Science & Engineering and titled "Process-Structure Linkages in Materials via Deep Learning from Phase-Field Simulation Data," has been reviewed in final form. Permission, as indicated by the signatures and dates below is now granted to submit final copies for the College of Graduate Studies for approval.

Major Professor:	Samrat Choudhury, Ph.D.	Date
Committee Members:	Indrajit Charit, Ph.D.	Date
	Mark Roll, Ph.D.	Date
	Vishnu Boddeti, Ph.D.	Date
Department Administrator:	Erik Aston, Ph.D.	Date

Abstract

Material microstructure is key to understanding processing-structure-property relationships. However, limitations in computational descriptions of microstructure present a challenge in being able to predict property changes under noisy processing conditions. Correctly modeling microstructure and being able to produce reliable material property predictions would enable efficient strategies for material optimization. Such strategies are shown to drastically reduce the amount of experiments needed to reach an optimal material. This in turn would decrease the time to market required to develop new materials, a key goal of the material genome initiative.

In this work, a general mechanism for linking processing, structure, and properties is developed through the use of Deep Learning. Two separate models have been developed. The first model, the encoder-decoder model, is used to link processing conditions to microstructure, while the second model, the predictor model, is used to predict material properties given the current material microstructure. The trained encoder-decoder model is shown to predict the non-trivial evolution of ferroelectric domains in bi-crystalline lead titanate perovskites. In addition to small constant inputs such as the processing temperature, the encoder-decoder can account for spatial input conditions, such as the arrangement of grains in a polycrystalline material. The predictor model uses the ferroelectric microstructure to predict the ferroelectric switching constant, the coercive field. It is demonstrated that the predictor model is able to model the coercive field property using only the microstructure with a similar level of accuracy as state-of-the-art machine learning methods that have been trained directly on input processing conditions. Even if the input conditions are unknown or noisy, the microstructure can often be observed accurately.

Further, the model has been demonstrated on more complicated environments with stochastic poly-crystalline systems. It is shown that the model is able to sufficiently capture and reproduce key characteristic features of the microstructure, despite never being

explicitly programmed to do so. The overall volume fractions of domains is maintained, the formation of domain walls occur along directions expected analytically, and the polarization is reduced along grain boundaries in the presence of a secondary phase.

Acknowledgements

It has been my privilege to work with Prof. Samrat Choudhury, who has provided me with the support I needed to meet the objectives of this work. I will remember his helpfulness as an academic adviser and encouragement to continue to aim higher.

Prof. Vishnu Boddeti has been a great source of guidance for the technical aspects of my work and I would like to thank him for providing his expertise in machine learning.

I would like to express sincere thanks to Prof. Mark Roll for his excellent guidance and support during this master's project. His continual faith in my abilities and prompts to push me a little further have been a great source of confidence. I will always remember his constant support, encouragement, suggestions and valuable comments. In every aspect of my work he has made himself available as a great source of inspiration and scholarly conversation. Without his encouragement and keen words of recommendation in all of my endeavors, this would have been an impossible task.

I would like to thank Prof. Indrajit Charit, Prof. Krishnan Raja, and Prof. Batric Pesic for being excellent sources of information and invaluable mentors. I owe my foray into the world of Materials Science to these great gentlemen, and their ability to never miss an opportunity to indulge a passing student's curiosity.

I gratefully acknowledge the financial support provided by the National Science Foundation through the Graduate Research Fellowship Program for making this degree a possibility through its generous funding. I thank the Graduate and Professional Students' Association for awarding me travel grants for presenting my work at TMS 2018. [1]

[1] Any opinion, findings, and conclusions or recommendations expressed in this material are those of the authors(s) and do not necessarily reflect the views of the National Science Foundation.

Dedication

I would like to dedicate this work to my mother, for her unwavering confidence and support throughout my academic career, and to Kylie Touchstone for her fantastic input, love and encouragement.

Table of Contents

List of Tables

List of Figures

Chapter 1: Introduction & Background

1.1 Motivation and Justification

In the course of human history, each era of mankind's progress has been best described by the materials used. The first humans made use of bones and wood for hunting. During the following 3 million years of the stone age, shelters were built and basic stone implements were used in the collecting of food. The introduction of metallurgy starting with the bronze age and improving through the iron age in around 1000 BCE gave rise to tools capable of improving the quality of life. From there, with metal working and improved tools, a cascade of improvements followed over a relatively short time period in human history. The production of metals and the study of alloys was followed by technological leaps in glass working, ceramics, and polymers building momentum until the industrial age in the 18th century.

Progress continued at an even greater breakneck pace than before, driven by the sharing and accumulation of knowledge gained through both successful and failed experimentation. The 20^{th} century saw the development of phenomenological models now seen as pillars of materials science, including the renowned Hall-Petch relationship [1] and the Hume-Rothery rules [2]. These arose from iterative experimental work on alloy design and became invaluable in the creation of future materials.

Today, materials science and similar fields benefit greatly from the presence of computers that now play an integral role in handling and processing knowledge. Since the introduction of the supercomputer, they have run material simulations, starting with the first molecular dynamics in 1950s. This trend continued with the emergence and growth of quantum mechanical methods, including the ubiquitous density functional theory for *ab initio* atomistic simulation [3]. Other methods developed from thermodynamics, such as phase-field method which was used to predict dendrite growth [4]. These simulations helped

realize new breakthroughs in experimental technologies, which led to further improved simulations.

The development of many distinct computational methods that are each useful to a particular time and length scale has led to an effort to combine many different methods to simulate macroscopic behaviour with the accuracy of *ab initio* quantum mechanics. This effort is referred to as multi-scale modelling [5]. Many details in materials science are a direct result of many scales, from point defects on the nanometer scale to compressive stresses on the centimeter scale. Figure 1.1 demonstrates how many different length scales interact to form a cohesive material property and affect the overall properties. Being able to observe many timescales simultaneously is one of the many advantages of computer simulation.

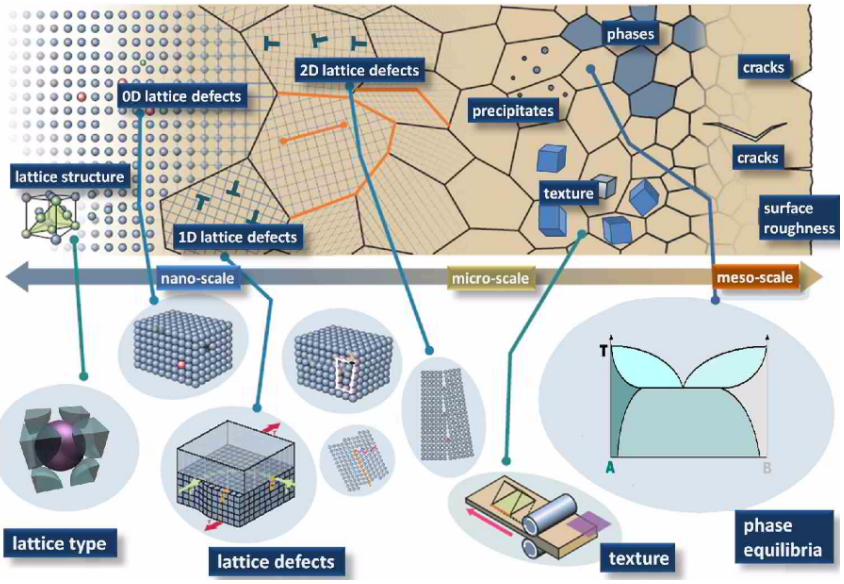

Figure 1.1. A schematic of many different defects and considerations that occur on a wide range scales in materials science [5].

The widespread availability of computing power combined with the advances in theoretical physics has created the era of computational materials science. The advent of quantum mechanics and density functional theory has allowed powerful computing software to simulate individual atoms and atomic force-fields. However, much of this research, both

experimental and theoretical, could be collected into a database for further use. Current practice is to perform necessary simulations and experiments to emphasize a particular research interest. The data is used to generalize information and findings but is not typically made available in an accessible searchable manner. Today, one of the challenges is to create large databases where research knowledge is collected and processed. With such databases, materials can be filtered and trends identified. Ultimately, as seen in the similar fields of bioinformatics and cheminformatics, the ability to generate, process, and retrieve data efficiently from many sources is critical to developing a rapid development cycle. Likewise, **materials informatics** is an upcoming field that aims to create high quality experimental and computational databases with the goal of applying modern machine learning techniques and data mining methods to evolve new models [6, 7]. Once a knowledge base is established, many data-driven tools become useful, such as those in machine learning.

1.1.1 Material Informatics

Material informatics databases have already began evolving. In 2011, the Materials Genome Initiative [8] was created as a direct parallel of the Human Genome Project [9] in an effort by the US Government to "discover, manufacture, and deploy advanced materials twice as fast, at a fraction of the cost." Other projects have sprung up, such as the Integrated Computational Materials Engineering (ICME) [10], and the Advanced Manufacturing initiative [11], the Materials Project [12], and AFLOW [13]. Even more recently, an Executive Order has been announced to maintain "American Leadership in Artificial Intelligence" with the aim of increasing adoption and use of data science across diverse scientific fields [14]. Such initiatives brought about a number of methods from information statistics to jointly optimize materials through machine learning. One major challenge of materials design is determining the optimal composition and processing to obtain desired properties. Prior to recent years, time-consuming Edisonian trial and error

was the norm. The powerful combination of machine learning methods, high-performance computing, and modern databases displays great promise to revolutionize the development process, lower processing costs and accelerate the pace of materials discovery.

Recently, theory has become powerful enough to accurately predict materials characteristics. Even with these advances, the sheer combination of possibilities in the parameter space, even with logical elimination of poor choices, the materials landscape is far too large to compute. Thus, it has been found that the best approach may be an iterative approach that learns from available data using statistical inference. The typical optimization process consists of 1) develop a model that enables prediction of property y from x materials, 2) utilize these models to predict the optimal x to synthesize next, and 3) measure y from this new x material and add the new dataset to a database. Step 3 provides difficulty as a factor of the arduous process necessary to synthesize a new material and accurately measure a known property. Therefore, it becomes productive to synthesize as few compounds as possible to remove the bottleneck.

At the forefront combining statistical inference with high-throughput is an approach known as adaptive design strategies using uncertainties [15]. Machine learning advances have shown that picking the best predicted option from the regressor may not be the optimal choice when the predictions have associated uncertainties [16]. This is particularly important when small data sets are used to extrapolate to large unexplored chemistry search space, such as in materials design. Instead, an additional model is used to measure the errors associated with the prediction, and choose the next material that maximizes the "expected improvement", which depends on both the predicted properties and the predicted error associated with them. This method is very useful, as it can balance exploration and exploitation of the data. Here, exploration is the wide searching of many very different possibilities, while exploitation involves iterating over similar possibilities. During initial modeling, exploration is very important to identify many different possibilities that may be more optimal. However, as the model approaches the targeted property, exploitation

becomes the driving factor. Two excellent algorithms for this method are Efficient Global Optimization (EGO) from 1998 and Knowledge Gradient (KG). Both algorithms have enjoyed widespread success outside the field of materials science, especially in process design, and can be used effectively to escape local optima. These algorithms optimally choose between the tradeoff of exploiting the materials closest to those giving best results and exploring completely new materials. Additional exploration will add to the overall dataset and improve the quality of the predictions. Overall, adaptive design is a powerful general method to select the next best material to test.

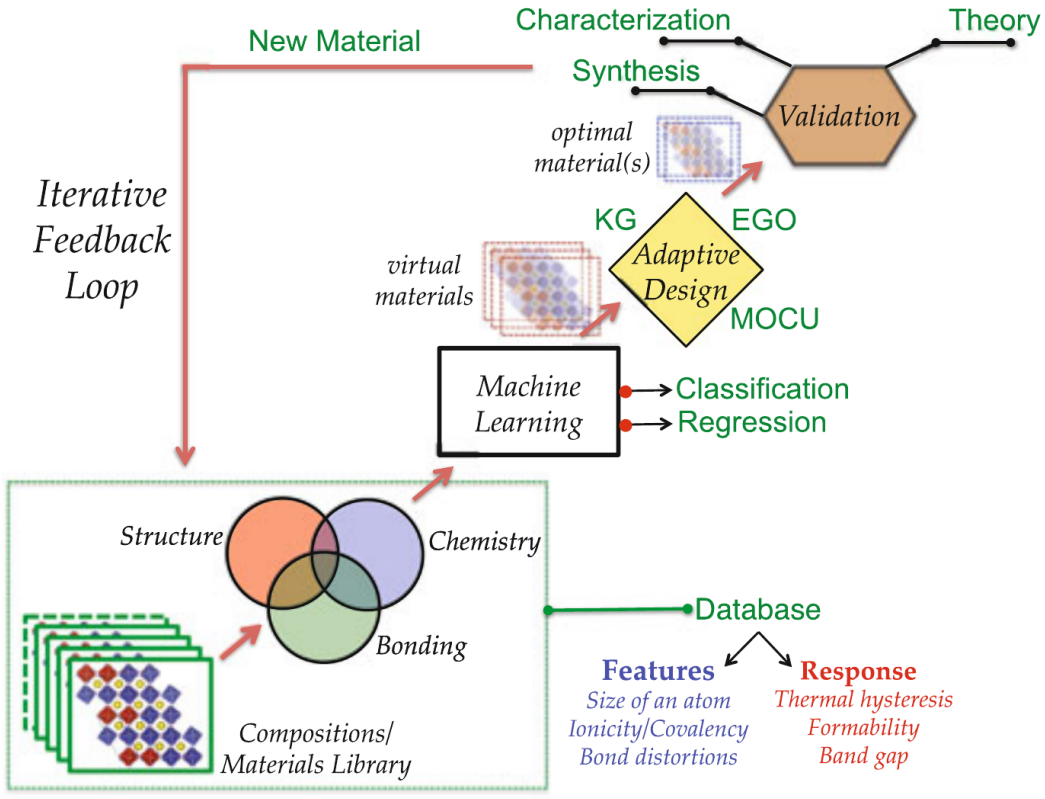

Figure 1.2. A schematic design loop showing adaptive design strategies that incorporate machine learning with iterative feedback. KG, EGO, and MOCU stand for knowledge gradient, efficient global optimization, and mean objective cost of uncertainty, respectively [6].

Figure 1.2 demonstrates the basic design principles of adaptive design. A database involving many different characteristics and features of materials is used to train a classifier

(a tool to predict what category the data belongs to) or a regression algorithm that chooses the materials it predicts should provide the best properties. Out of theses predicted materials, an adaptive design algorithm chooses the material that has the maximum expectation based on the error in the prediction process. This material is selected for further validation and testing and eventually gets added back to the database. This process can drastically decrease the materials testing necessary to reach new optimal materials.

Adaptive design strategies have garnered utilization in high-throughput methods to optimize material chemistry [6]. This in combination with the popularization of density functional theory directly lead to chemistry optimization capably being performed and screened computationally. There have been many strategies utilizing modern optimization techniques for solving the chemistry as a black box function [15]. Density functional theory allows bulk characteristics of crystals and defects to be calculated with relative ease. However, there are few studies that aim to quantify and utilize the microstructure of a material, despite the advantage presented in experimental works. Data-driven materials design has been applied successfully to materials chemistry challenges, but there still are many challenges that need to be solved before the same can be applied to optimize the structure of materials. Materials structure, specifically microstructure plays a major role in defining material properties.

A common paradigm ubiquitous in materials design is creating understanding of processing-microstructure-properties (PSP) relationship for a given material. This focus is ideal for creating key concepts in engineering new materials and focuses on the processing conditions to create a material, the microstructure that defines the material, and the properties obtained [17]. However, in practical applications the materials contain many different phases present on a microscopic scale that are linked with drastically different properties.

Material properties, such as tensile strength, elongation, fatigue life, creep life, and toughness ultimately depend on the arrangement of these microstructural features, which

in turn arise from a combination of the processing conditions and operating conditions the material is exposed to. To better understand the properties of the microstructure, phenomenological principals such as the Hall-Petch relationship are commonly employed to link them to both the processing conditions and the properties of a material. These models ultimately fail to capture the relationship between the process-microstructure-property relationship. Chemical analysis in combination with phenomenological models can only provide pieces of the full understanding necessary to optimize material properties. A more complete understanding can be developed by recognizing features present in the microstructure. Unfortunately, the microstructure has remained a difficult object to quantify and learn from. With the aid of machine learning, it is possible to digest visual microstructure characteristics and in turn, relate them to properties.

1.2 Machine Learning Concepts

Machine learning is a field pioneered by computer scientists that gives computers the ability to learn and predict without being explicitly programmed [18]. As a result of this lack of needing explicit programming, it is a powerful tool that can explore the construction and variation of algorithms that can make predictions from data. Typically recognized as a subset of artificial intelligence, machine learning includes the subfields of data mining, unsupervised learning, and predictive analytics. Machine learning is limited by the methods of pattern-finding available, the scope of the parameter domain, and quite nearly always by the training data available. These pitfalls are commonly overlooked and lead to machine learning algorithms failing to deliver.

Conversely, it has been shown that machine learning works quite well when applied to suitable branches of science within a narrow, well-studied domain. The example cases of bioinformatics and cheminformatics are a testament to the true power of machine learning in science [19–23]. In material informatics, as it was in other fields before it, the struggle is primarily due to a dearth of expertly labeled data in a coherent collection. Many efforts are

currently on-going to coordinate data curation that aim to fix this issue in the long term. Materials science has built up large amounts of data available in publications over the last decades dealing with many critical problems. However, collecting that information into cohesive relational databases is a task that requires significant community contribution and coordination. In many cases, sufficient data has not been provided and overfitting, can occur on small sample sets. For the work prepared in this document, much of the data was able to be generated on a personal computer. This allows us to develop prototypes that can be leveraged later on as new data collections are built.

Machine learning is typically classified into two broad categories. The first is unsupervised learning, in which no labels are attached to the input data and it is expected to find a structure inherent in the data. A label is simply an attribute of the data without human bias. For instance, given an image of aluminum microstructure, a label could describe its composition, or processing conditions, or even just the type of alloy. Unsupervised learning is a powerful form of learning that can lead to many patterns and trend analysis in the data.

The second category of machine learning is supervised learning, during which the computer is fed a series of inputs which correlate to specific outputs and its objective is to predict the output. The supervised learning domain can be further dissected into classification and regression problems. In classification, the inputs are segregated into discrete classes and the learning device must model that assigns inputs to one or more of these classes. For instance, one might show a model pictures of different types of animals and expect the desired output to have the highest score. Regression is another common type where the outputs are continuous, rather than individual groups. To build a system that can predict the cost of homes, one would first collect information about the houses being sold, such as the location, square feet, rooms, etc. During training, the machine learning algorithm would be fed this information and the output would be expected to be as close the actual sale price as possible. Although it is sometimes possible to model

classification as a regression problem by assigning the classes to a number and trying to regress between them, this method makes the underlying assumption that there is a linear relationship between the classes and that the ones following a class may be closer than the rest.

During the training process, we compute an objective function (also called a loss function if it should be minimized) that measures the error (or distance) between the output scores and the desired scores. The machine modifies some parameters internally in such a way to reduce this error. These parameters are often called weights and are real numbers that define the relationship between the input and output. For instance, in the house price prediction example, the loss function could simply be the difference between the actual selling price and the predicted selling price. The objective function can then be seen as a hilly landscape, one with many valleys of differing depth [24]. Although the objective may be to identify the deepest valley, it can be easy to get stuck in more local minima. Furthermore, the shape of the "landscape" can change drastically depending on the data available.

The limitation of this available data provides some interesting problems. It is possible for a model to generalize poorly where it exhibits bad performance on data it has never seen before, but do extremely well on the data that it was trained with. This phenomenon is known as over-fitting. Solving over-fitting is a sub-field of its own, but typically a close solution can be found through limiting the number of parameters and regularization. Over-fitting is a problem particularly relevant in the field of materials science where experimental data is costly. Figure 1.3 provides an overview of how the data-driven design philosophy applies to materials science. There are many avenues of data creation and generation.

Despite the difficulty involved, machine learning aspects of the process-structure-property linkage can provide new insight and automate the material selection and screening process. Many mechanical properties, such as yield strength, fatigue life, creep life, and

toughness result from the microstructure of a material. Regression methods have provided a foundation for modeling chemistry-property relationships in materials science [6, 15, 25]. However, these methods often fail to take into account the nature of defects, secondary phase particles, grain boundary interactions and other features that take place on the scale of the microsctructure. Experienced metallurgists often understand that by observing the microstructure, they can target processing parameters to see their desired properties. For example, for steel it is understood that the coexistence of more microstructural features can lead to decreased crack propagation and increased fatigue life. Such qualitative measurements are difficult to attribute to any single change in processing parameter and introduce bias into the characterization process. Bias is introduced as an expert is required to first recognize and identify key microstructural features. Despite recent advances in microstructure recognition and analysis, the field depends heavily on expert knowledge to identify features of interest for quantification. Therefore it is desirable to explore methods of analyzing and predicting microstructure in a quantitative fashion which do not require *a priori* knowledge of features of interest to automatically pick features that have the most impact on properties.

To address the concerns presented by machine learning microstructure, new tools are needed that are capable of processing image data in an efficient manner. Neural networks are a strong component of machine learning that have gained traction in recent years and shown great progress in images and multidimensional data.

1.2.1 Neural Networks

An artificial neural network consists of multiple layers each filled with computational units called *neurons*. Each neuron takes a set of inputs from the previous layer (the first layer being the input to the network) and multiplies it by a weight and shifts it by a bias. It then applies an *activation function* to map the value over a nonlinear space, and the resulting output or *activation* is passed to the next layer. Figure 1.4 demonstrates the

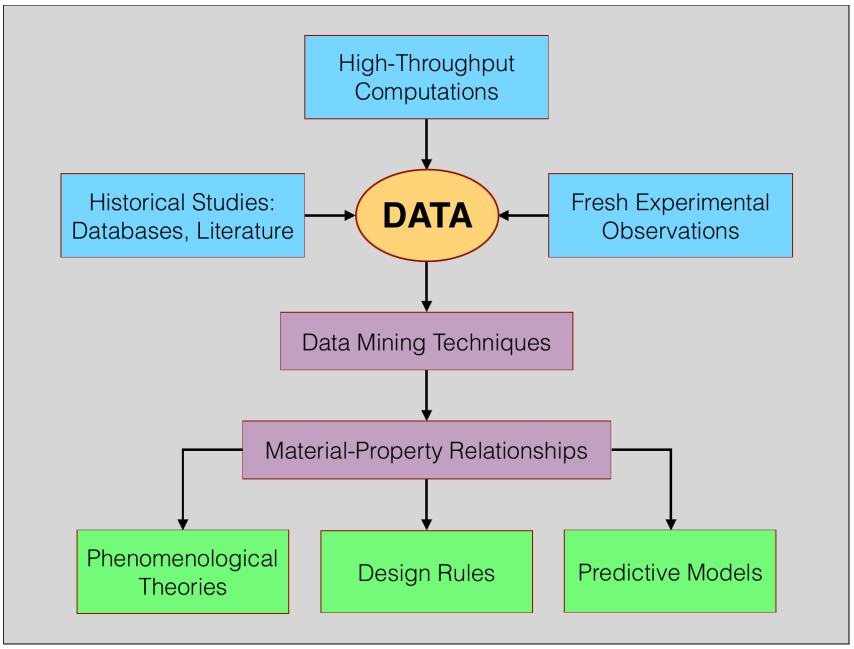

Figure 1.3. Schematic detailing data-driven materials design philosophy [26].

basic topology of a simple neural network consisting of a single hidden layer.

In this basic fully-connected state consisting of neurons that are fully connected to each neuron of the next layer, neural networks are hard to train and grow computationally prohibitive as the network size increases [28]. There have been many adaptations to the basic principles in an effort to decrease the drawbacks of neural networks. These adaptations take the form of better activations functions, loss functions, dropout, regularization, convolutions, and other ideas that have been incorporated into modern network designs.

In training networks, it is often desirable to produce an algorithm that performs well on not just the training data, but also on new inputs. Regularization is a method used to decrease the test sample error even at the cost of increased training error. Through regularization, the algorithms can be tuned to perform better for a specific objective. One of the most common kinds of regularization is the L^2 parameter norm known as weight decay. This strategy encourages weights to be near to the origin by adding a term to the loss function [29].

Activation functions are applied to the output of the neuron. These activation functions

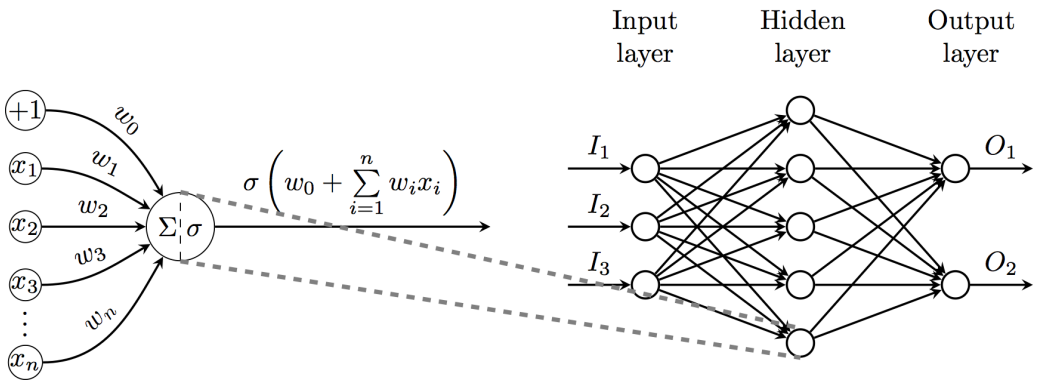

Figure 1.4. (left) A neuron with inputs x, weights w_i and activation function σ with bias w_0. (right) A neural network with one hidden layer [27].

are necessary so that the network does not become a linear function of its input. The most common activation function today is the rectified linear unit or ReLU defined by $g(z) = max\,(0, z)$ [30]. This function is piecewise linear, as it maintains its linearity for positive values but is 0 otherwise. Because of this near linearity, rectified linear units are able to preserve many properties that make linear models easy to optimize.

Today, networks in which a neuron in one layer is connected to each of the neurons in the next layer (fully connected networks) are rarely used directly for image analysis. Due to a very large number of parameters, fully connected layers are difficult to train and further require an extraordinary amount of computer memory. Instead, other options have been investigated to great success, such as convolutional neural networks, which outperformed every other method in the 2011 ImageNet classification competition [31].

1.2.2 Convolutional Neural Networks

Convolutional neural networks (CNN) have been recognized in recent years as state-of-the-art for computer vision tasks [32]. A CNN is a specific type of artifcial neural network that can utilize layers with convolving filters (called *kernels*) that are applied to local features [33]. Essentially, a CNN is a neural network that uses convolutions in place of general matrix multiplication in at least one of their layers. Figure 1.5 presents an example of a kernel sliding along an input image to produce the next layer of output. The output

of such layers are called convolution maps. Convolutions are important as they leverage sparse interactions, parameter sharing, and equivariant representations. Convolutions also provide the very important benefit of being able to deal with varying image sizes.

In a traditional neural network, every output unit interacts with every input unit. Convolutional networks typically have sparse interactions by making the kernel smaller than the input layer. The input image may have millions of pixels, but small features such as edges can be detected with kernels of only tens of pixels. This has the advantage of lowering the number of parameters and correspondingly lower memory costs. Fewer parameters to optimize also means a more stable and statistically efficient system. Neurons in deeper layers of a convolutional neural network may indirectly interact with more of the greater image. This allows complex interactions and features over large range-scales to be taken into account.

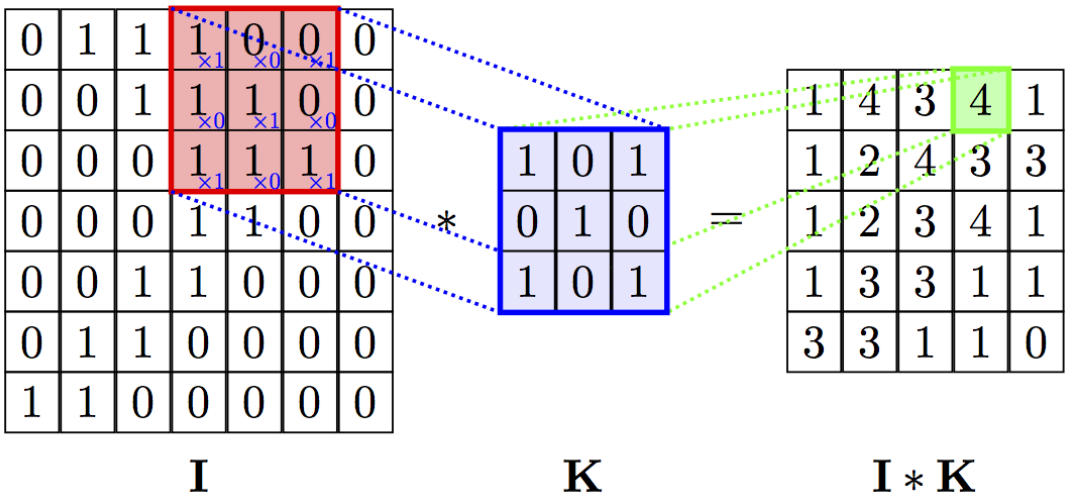

Figure 1.5. A two-dimensional convolutional operator demonstrating the kernel K sliding across the input image I to produce $I \cdot K$ [27].

Parameter sharing is another equally important advantage of CNNs where the same weight is tied to the value of weights elsewhere. In the instance of convolutions, each weight of the kernel is applied to every position on the input layer. This implies that much fewer parameters are needed to obtain useful information about the layer. Specifically,

convolutions have a particular form of parameter sharing called equivariance. That is, as the input changes, the output will change in the same way. A function $f(x)$ is equivariant to function g if $f(g(x)) = g(f(x))$.

A convolutional network layer typically consists of three steps. First, the layer performs many different convolutions on the same input image with different kernels to produce a set of linear activations. Second, these linear activations are passed to a nonlinear activation function, such as the rectified linear unit. Finally, a pooling function is used to coarse grain the image. During pooling, a statistic is taken over a small region of the input layer, such as the maximum in a 3×3 pixel region. Through this process of convolving and pooling, CNNs develop knowledge of very complex correlations over large length scales which makes them an ideal candidate for image recognition and microstructure analysis.

1.2.3 Challenges with Microstructure

The applications of large multilayer neural networks are limited in their capacity to many scientific fields as a result of the requirement of large amounts of training data necessary to prevent over-fitting. Neural networks often require 100,000s of training samples to generalize to a large enough subset. As of this time, there are no materials databases of that magnitude publicly available. As a result, using pre-trained neural networks via transfer learning is often preferred [34–36]. Transfer learning is a process where a network that has been trained for one task gains inherent knowledge about the images or features it is sampling that can be used to describe features in completely unrelated tasks. These transfer learned neural networks may not perform as well as a network trained with the intention of microstructure analysis. The transfer learned process relies on non-specific information as well as some form of dimensionality reduction. They present a very limited ability to analyze the microstructure and the analysis cannot be reversed currently (the transfer learned network could not predict a microstructure from a desired property set). Furthermore, current networks are trained for two dimensional image classification.

Electron backscattered diffusion and other microstructure analysis methods produce three dimensional observations of a sample which are required for a complete analysis. Transfer learned methods would not be able to process higher dimensional images and much of this information would be lost.

1.3 Data Generation Methods for Machine Learning

In order to build a model, neural network or otherwise, first there must be data. There are many apparent sources of data that could be applied. Ideally, this would collect and condense many multifaceted research efforts into one large database to make extensive use of real-world data. However, many good simulation tools exist that can provide a stepping stone to prototype and test models without resorting to expensive and time-consuming experimental methods. These tools provide results within a reasonable accuracy of experimental methods and contain many of the necessary complications seen in experimentally. This makes them much better suited than many of the toy problems models are currently tested on, such as Gaussian Random Field [37]. Although noise algorithms produce a somewhat detailed microstructure, this pseudo-microstructure lacks the long-range interactions typically observed.

The recent trends in computational materials science have largely been accomplished through high-throughput simulation techniques. The most accurate of these simulation methods are based on quantum mechanics (QM) such as ab initio post-Hartree-Fock chemistry and quantum Monte Carlo (QMC). Such simulations are able to ascertain a number of useful bulk material properties, including atomic crystal structure, equations of state, melting points, elastic moduli, defect formation energies, and many other properties. However, the usefulness of QM methods is limited at larger length scales and it is unable to calculate properties that arise as a function of long-range behavior, such as plasticity in metals, polycrystalline behavior, particle coarsening, and grain boundary inclusions.

Multiple methods of simulation are necessary to form a more complete analysis of the material.

Larger scale methods such as molecular dynamics or phase-field require experimentally derived energies and fields and may altogether make assumptions that are invalid for the given material. Together, the techniques may be employed jointly to develop a multiscale model. In the following sections, we discuss different techniques to generate data for machine learning at different length scales.

1.3.1 Density Functional Theory

Density functional theory is one of the most popular quantum mechanical approaches to date as it can potentially calculate very accurate results, but at high computational cost. It is considered an *ab initio* method, derived directly from theoretical principles with no incorporation of empirical parameters or experimental data. However, common practice is to use functionals that are derived from empirical data. It is used to determine the electronic structure, or the probability distribution of electrons in materials. The electronic structure is obtained through the solution of the Schrödinger equation associated with the Hamiltonian. The molecular orbitals are determined through an iterative process of assuming static atomic positions and finding an approximate solution to the wavefunction. Once a solution to the wavefunction is found, the gradient is used to update the positions of the atoms. The gradient is determined by taking the derivative of the total energy with respect to the position of the nuclei. DFT expresses the total energy in terms of electron density, rather than explicitly through the wavefunction and provides a viable alternative to post-Hartree-Fock methods for large systems.

As a result of its low computational costs and accuracy, DFT is considered a de facto standard for atomic simulations today. It is accurate enough to be directly comparable with experiment in many cases [38]. However, it is limited in the number of atoms that can be reasonably observed; DFT is limited to a scale of a few dozen atoms. This limits

its ability to observe macroscopic phenomenon. Furthermore, without cluster expansion and *ab-intio molecular dynamics*, DFT cannot observe kinetically limited reactions. DFT requires large amounts of memory and requires a small supercomputing cluster to obtain results in a reasonable time frame. Calculations can take as low as a few minutes for bulk calculations to tens of thousands of CPU-hours for more complex systems. Furthermore, calculations of band gap in semiconductors and some intermolecular interactions (such as van der Waals forces) are difficult to calculate with DFT. Overall, DFT is an extremely popular tool to date for calculations in solid-state physics, but it is limited on length and time scales. However, information from DFT can be used in other methods suitable at larger length scales, such as molecular dynamics or phase-field modeling.

1.3.2 Molecular Dynamics

Molecular dynamics (MD) was one of the first simulation methods pioneered by Alder and Wainwright and Rahman in the late 1950s and 1960s. It has since been widely adopted as a staple tool in many areas of physics and chemistry [39]. Classical MD treats atoms similarly to the "ball and stick" model. Atoms are soft balls with elastic radial cutoffs that correspond to bonds. With the right applications of force fields derived experimentally or from QM theory, classical MD can be very powerful. It is capable of modelling millions of atoms simultaneously. It is capable of modeling the evolution of a system over small time scales. This is extremely useful in many fields, particularly molecular biology.

As mentioned briefly earlier, *ab initio* quantum mechanics based schemes are rising in popularity due to their accuracy and efficiency. However, DFT cannot access timescales larger than a nanosecond. In this regard, the field of quantum MD has been developed. Quantum MD uses the ingredients from quantum mechanical theory, such as the potential energies and atomic forces. However, the evolution of the atoms is performed classically. This allows MD to retain *ab initio* accuracy while still performing temporal evolution on many atoms [40].

Like other simulation methods, molecular dynamics is limited by the choice of potentials and interatomic forces. Molecular dynamics is able to simulate much larger length scales than DFT, allowing it to observe much more complex systems. However, quantum MD faces a trade-off of accounting for all valence electrons and system size. Further, quantum MD techniques are still limited to the ground-state adiabatic surfaces. The most severe problem for MD is the limitation of time-scale, which requires very small integration steps which makes modeling processes that take microseconds or even seconds very difficult.

1.3.3 Phase-field Modeling

Phase-field modelling is a powerful mathematical tool for solving mesoscale interfacial problems [41]. It has previously been employed to predict 3-D microstructure evolution kinetics in many diverse material processes, such as ferroelectric and ferromagnetic phase-transition, phase-separation, solidification, precipitation, and twinning. It is based on fundamental thermodynamic and kinetics and is able to model the temporal evolution of the microstructure [41–45]. Phase-field does not require any prior assumptions of the microstructure morphology, and it does not explicitly track the location of interfaces. Furthermore, phase-field can efficiently perform 3-D representations of material processes with both short and long range interactions [46].

A very recent case leveraging the advantage of phase-field modelling can be seen in the field of irradiated nuclear materials [47]. Atomistic methods, such as DFT, molecular dynamics, kinetic Monte Carlo, cluster dynamics, and rate theory, have been employed to determine the thermodynamic and kinetic properties of irradiation defects. However, it was seen that these combined methods still face significant challenges in determining properties such as hardening and ductile-brittle transition temperature due to their reliance on microstructure. In this case, the phenomenon happen on a length scale between nanometers to micrometers and important processes occur in femtoseconds but cascade over years. Phase-field is uniquely suited to these problems to cover the temporal evolution

over larger scales [47].

However, phase-field is not without its own unique set of limitations. The phase-field method relies on accurately experimentally determined constants. The error accumulates with the error in these constants. These constants are often difficult and expensive to measure and the systems which can be observed are limited to measured and published values. Furthermore, phase-field, like other non-*ab-initio* methods, is limited by the systematic description and mathematical formulation of each defects it wishes to encompass. As a result, the phase-field method typically only provides qualitative and semi-quantitative answers as an observation of trends. Most real processes are much more complicated than what is modelled by phase-field, and only a limited set of energies can be taken into account. As a result, the trend is captured, but not physical values. On the accuracy of phase-field, as a continuum level technique, each grid point cannot represent smaller than one lattice point, as it cannot resolve features smaller than the lattice parameter. Despite these limitations phase-field has been used successfully to model a large variety of problems in materials science and offers a tool to observe the evolution of heterogeneous microstructures. It offers a computationally efficient method for observing real trends and features at the continuum scale.

1.4 Ferroelectric Materials & Microstructure

A **ferroic** is a material that adopts a spontaneous, switchable internal alignment. Despite the name, few ferroic materials contain any iron at all. Figure 1.6 shows the primary ferroic parameters and the relationship between them. A ferroelectric material is a type of ferroic in which an electric field induces a switch in the electric dipole-moment alignment. Ferroelectrics are of considerable interest due to their high-ranging applications in electronic and electro-optical devices, such as acoustic sensors and actuators [48].

More specifically, a ferroelectric can be described as an insulating system with two or more discrete states of different nonzero electric polarization in zero applied electric field

[49]. This persistence of polarization without the presence of an electric field is referred to as "spontaneous" polarization. This region of spontaneous polarization with a uniform direction is known as a **ferroelectric domain**. A system considered ferroelectric must be able to switch between these states of alignment in the electric dipole-moment with the presence of an applied electric field.

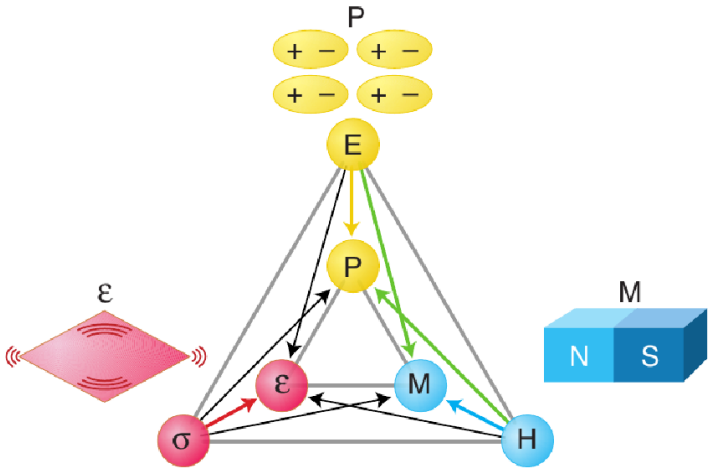

Figure 1.6. Diagram of the relationship between the ferroic order parameters. The electric field E, magnetic field H, and stress control the electric polarization P, magnetization M, and strain ϵ, respectively [50].

The key concept in understanding ferroelectricity is to develop an intuitive grasp of electric polarization. For a defined system of constant volume, the electric polarization P is defined as

$$\vec{P} = \frac{\mathrm{d}\vec{p}}{\mathrm{d}V} \tag{1.1}$$

where $\vec{p}$ is the dipole moment, obtained from the charge density, and V is the system volume. However, for an infinite crystal, this definition is not valid. For an infinite crystal, the polarization is identified as an integrated current through a transformation from one variant to another, and is expressed as a Berry phase. In this formulation, the polarization is not a vector quantity, but a lattice.

Switching between alignment states is understood to take place on a scale larger than

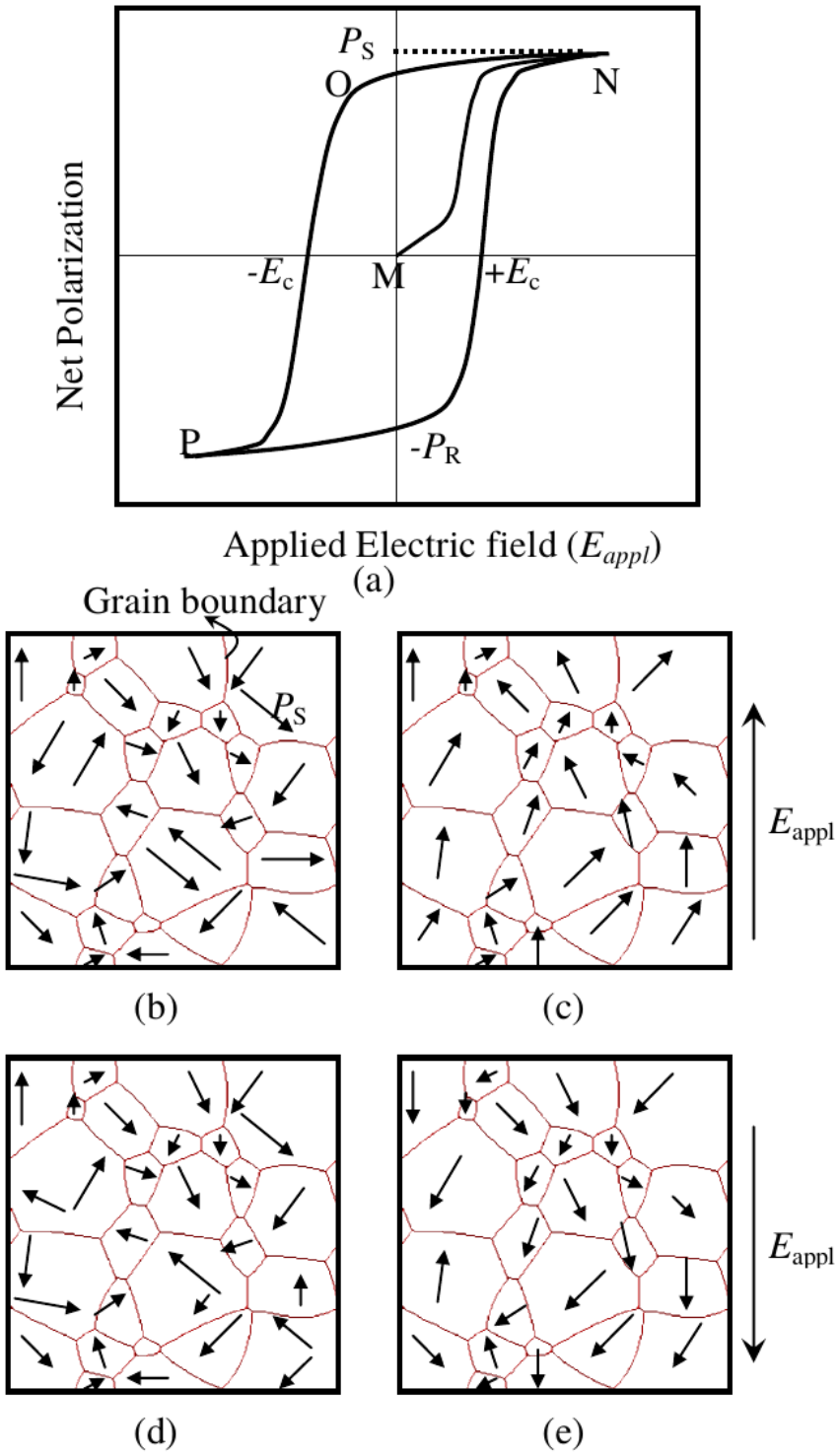

Figure 1.7. (a) A typical polarization curve for a nonlinear dielectric. P_s is the saturation polarization, E_c is the coercive field [51]. (b-e) Schematic of the domain structure in a polycrystalline ferroelectric corresponding to the points M, N, O, and P, respectively [51].

the unit-cell. Switching is believed to occur by the movement of the domain wall and corresponding change in size of the domains. Figure 1.7 shows the common polarization hysteresis of a two-dimensional tetragonal material with four directions without an applied field. It can be seen to start with random polarization directions that get aligned as an electric field along the positive y direction is applied. At the top it reaches a linear zone where all the domains have aligned to be in the direction of the applied field or perpendicular to it. As the magnitude of the electric field decreases to zero, not all of the domains shift back to their original alignment. This creates the hysteresis affect where a non-zero polarization is now observed in the absence of an electric field. This retained polarization is called the *saturation polarization* P_s. As the electric field is applied in the opposite direction, the polarization eventually reaches zero. Although it was previously believed that the domain magnitudes (here in the $-y$ and $+y$) were equal in magnitude, it has been shown [52] that the domains in the perpendicular direction are still apparent in the material and represent the majority of the magnitude at this point. The electric field required to clear the polarization is called the *coercive field*. In this canonical form, the ferroelectric hysteresis loop is symmetric. Different phenomenon during repeated electric cycles can lead to a non-symmetric hysteresis.

The creation of a non-zero spontaneous polarization results from the arrangement of ions in the crystal structure. Two types of ferroelectrics discussed here are the conventional ferroelectrics where the position of the ions dictates the polarization, and electronic ferroelectrics which are dependent on charge ordering of multiple valences. For a nonzero spontaneous polarization to occur, the crystal must have a polar space group. However, the crystal must also be able to switch between different variants with an electric field, which drastically reduces the number of ferroelectric crystals. A small distortion of a greater symmetry through polar displacements coupled to the lattice strain is common [53].

The wide range of applications lends ferroelectric and multiferroic materials to be

a popular research focus of the last couple decades. However, despite their apparent popularity there still remains many unexplored avenues associated with their production and evolution. The complex chemical interactions and the microstructural domain evolution present within ferroelectric devices makes multiferroics and, by extension, ferroelectrics an excellent candidate for machine learning applications.

1.5 Thesis in a Nutshell

Computational materials science can enable much more efficient materials design and development. This work uses Deep Learning, a popularized term for artificial neural networks, to build a model that can ultimately connect processing-structure-properties solely using modern neural network methods without any explicit programming about the nature of the material being modeled. Producing an intelligent model that can predict material properties would help guide further exploration. A model without explicit programming is more easily adapted to new problems and does not carry any bias of an expert. However, such a model is difficult to design because not all processing parameters may be known, or are not known exactly (there is often noise in experimental data). Thus, predicting properties based on processing parameters alone is often insufficient. Instead, material microstructure may be assumed for ideal conditions and property predictions based on the idealized microstructure. This presents an alternative view where the microstructure that is derived from processing parameters is used to fingerprint the material properties.

To reiterate, the primary goal of this research was to use modern Deep Learning tools to establish a link between processing-structure-properties in a general form. To that end, the general outline of this document is as follows. Chapter 1 introduces the topics being covered in the remainder of this work. It briefly touches on the tools used, and outlines the justification for this work.

Chapter 2 discusses previous works with similar objectives and recent works that make use of deep learning.

Chapter 3 overviews the techniques used to produce the data and details how the models were created.

Chapter 4 presents a general model used to link processing conditions to microstructure in the case of bi-crystalline lead-titanate. It was trained using phase-field simulations. Further, a second model is presented that can link microstructure to properties.

Chapter 5 extends the general model to poly-crystalline microstructure. Furthermore, the model is shown to learn a weight of importance for the input. It is shown that different energetics contribute to different parts of the microstructure.

Finally, Chapter 6 summarizes and concludes the work while offering some directions for future work.

Chapter 2: Literature Review

The study and design of microstructure is ubiquitous in the field of materials science, but requires domain specific expert knowledge. Further complicating studies, microstructure incorporates many facets of materials science from large scale features observable with optical microscopy to small nano-scale strains to ferroelectric and ferromagnetic interactions. The defining feature of microstructure is the spatial inhomogeneity that separates a material from its pure defect free single crystalline counterpart.

Ivry *et al.* observed that microstructure in ferroelectrics is intriguing because it exhibits both long-range and short-range organization [54]. Essential microstructure information may include long-range interactions such as the distribution of ferroeleastic domains across neighboring grains. Shown in Figure 2.1, there are often patterns that form over a long range (distributed across several grains) that appear in microstructure. Capturing both long-range and short-range interactions is a difficult task to perform and often reconstruction algorithms are unable to do so without explicit programming.

Much of the challenge in identifying microstructure is the inherent stochastic nature of them. If, for example, one took an optical microscopy image of an aluminum sample and then moved the microscope to the left a centimeter and took another optical image, one would notice very similar characteristics between the two samples. They are, of course, the same material. They have similar properties, such as grain size distribution, grain shape, grain boundary width, and so forth. However, the images are completely different from a computer's point of view; the pixels are very different between the two.

To recognize the same microstructure despite very different pixels, the challenge is to identify the characteristic statistics of the microstructure (grain size, etc.) that define it and be able to produce equivalent microstructures that maintain these attributes. This task is commonly called Microstructure Characterization and Reconstruction. It incorporates techniques that provide some way to identify core components of microstructure and

methods to reconstruct material microstructure from an identifying fingerprint.

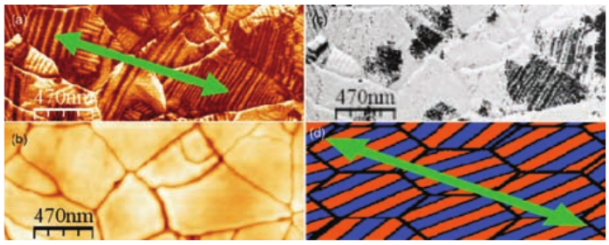

Figure 2.1. Long-range linear organization of ferroelastic domains from Ivry *et al.* [54].

2.1 Microstructure Characterization and Reconstruction Techniques

There are tools available to explore microstructure reconstruction and the relationship between processing, microstructure, and property. However, these tools are limited to very specific goals. A comprehensive review of current microstructure characterization and reconstruction methods is provided by Bostanabad *et al.* [55]; these can be categorized into the following:

1. Correlation function methods
2. Physical descriptor methods
3. Gaussian Random Field (GRF) methods
4. Markovian Random Field (MRF) methods
5. Deep Belief Network methods
6. Spectral Density Function (SDF) methods, and
7. Transfer Learning methods
8. Generative Neural Network methods

These existing techniques have limitations in their ability to link processing conditions to final microstructures. Methods 3, 4, 5, and 7 are based on rebuilding a target image, and do not have parameters to control the target based on processing conditions. The remaining methods (1, 2, and 6) involve a significant amount of information loss as dimension reduction is used to transform high-dimensional microstructure characteristics into a small set of key characteristics. This work implements and comments on the final method, a generative neural network (8).

2.2 Deep Learning Microstructure Characterization and Reconstruction

When this project was started, using generative neural networks was a novel idea that combined some of the best new technologies coming out of computer vision, machine learning, and materials science. During the creation of this thesis and throughout the research project, other works have emerged using deep neural networks in relationship to microstructure characterization and reconstruction. The works discussed here focus solely on characterization of microstructure and not on the relationship microstructure has to processing or properties. These are contrary to this work, which attempts not to characterize the microstructure, but to build a model to tie in processing parameters to microstructure and microstructure to properties.

Lubbers *et al.* [35] first used bilinear CNN representations to synthesize lamellar structures. This was the first known use of neural networks to generate microstructure-like features in materials science. They used a network previously trained on natural images (cars, people, birds, etc.) to capture the base texture of the microstructure, in a method known as *transfer learning*. Lubbers *et al.* demonstrated that neural networks seemingly are able to identify and reproduce the defining features of microstructure. In Figure 2.2, each image is passed through a neural network trained to classify natural images. Even though the network's classification metric is useless in the context of a

microstructure image, the network still parses many of the image features along the way. By extracting the activations at multiple layers in the network, it is possible to create a second image that matches those statistics. The result is a new microstructure that carries the same properties, but is ultimately different. This is one of the core challenges in MCR, identifying and preserving the statistics of the microstructure without explicitly programming all of the important features.

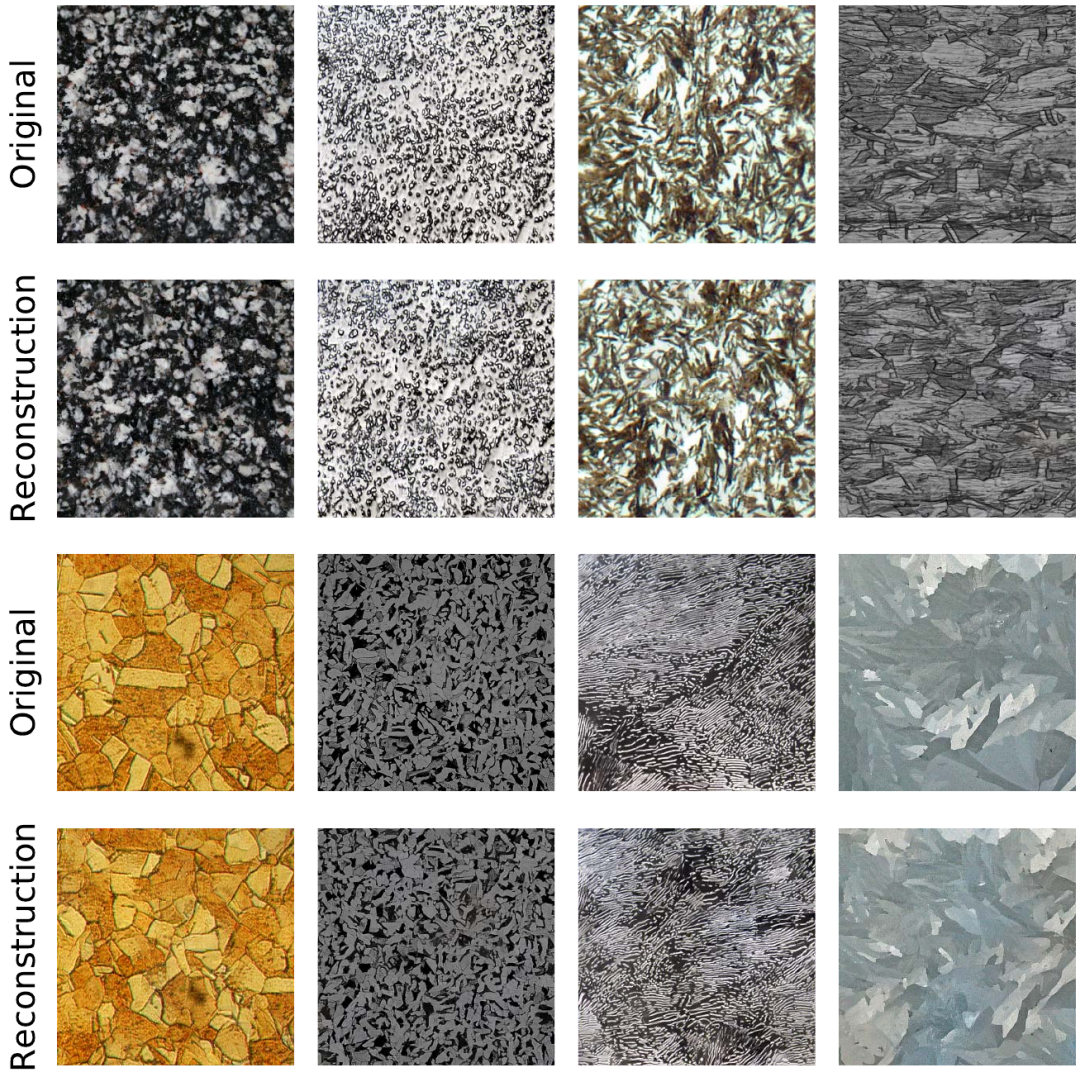

Figure 2.2. Texture synthesis of materials microstructure using a CNN. The CNN synthesizes each "Reconstruction" microstructure based on a single "Original" image. Reproduced from Lubbers *et al.* [35].

Lubbers *et al.* then generated a representative microstructure-like database using noise algorithms and show that they can reproduce the input parameters from the microstructure. This was done using dimensionality reduction across all the image statistics such that each image was passed through the pre-trained network and compared to every other image. This process is extremely costly and needs to be reperformed each time a new image is added.

Chowdhury *et al.* similarly used transfer learning to classify different dendritic morphologies on a self-produced database of experimental microstructures collected over the course of three years [34]. Decost *et al.* [36] analyzed 600 micrographs of high carbon steel and found that combining the statistics gained from transfer learning with a fingerprint achieved through vector of locally aggregated descriptors (VLAD), the classification rate was 98.9%. This method laid the path for identifying the presence of individual features at the microstructure level and using it to predict the relationship to properties.

Yang *et al.* produced a model for microstructure reconstruction using a similar technique to that used in this work [37]. Yang *et al.* chose to pursue a Generative Adversarial Network (GAN), which operates in a slightly different manner to the Variational Autoencoder (VAE) design used in this work. Details of the VAE will be discussed in the following chapter. The GAN design does not use a traditional loss function to compare the predicted microstructure to a real microstructure. Instead, a separate neural network component called a discriminator is used, as can be seen in Figure 2.3. The discriminator is learning to separate the fake microstructures from the real microstructures while the generator is attempting to learn to fool the discriminator. This allows the network to pick up core features without having identical images. Unfortanately, our early results showed that such a model did not perform well at high-resolutions. For more information, see Figure A.3.

Azimi *et al.* used a CNN without explicit coding of feature extractions to classify optical steel microstructures with an accuracy of 93% [56]. The categories were Martensite, Tempered Martensite, Bainite, and Pearlite. Kondo *et al.* used a similar comparison with

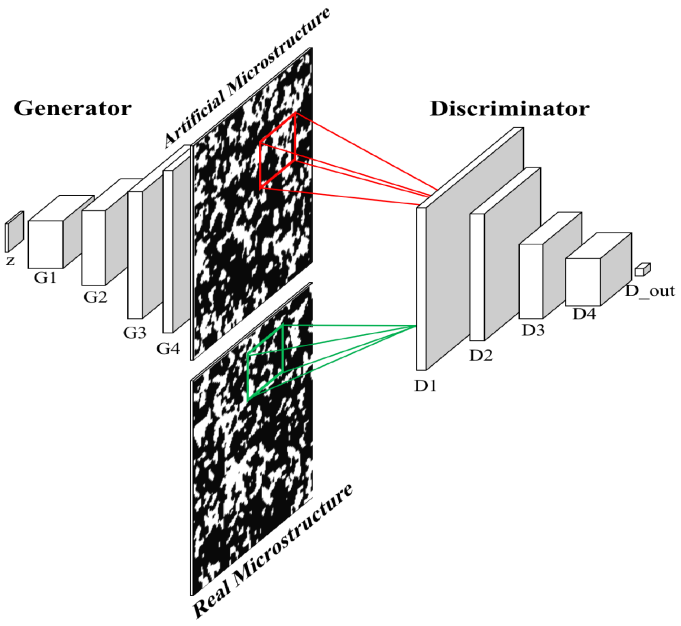

Figure 2.3. Schematic architecture of the GAN used in Yang *et al.* [37].

a CNN applied to ceramics to determine ionic conductivity [57].

2.3 Phase-field

The phase-field model is a mesoscale approach applied to understand the evolution of the microstructure in a variety of materials [41]. The phase-field model represents the state of the microstructure through a continous variable known as the order parameter ϕ. The order parameters changes diffusely across the domains or interfaces, and has a known width. This is directly opposite a mathematical representation with a sharp interface. Common variables used in the phase-field simulations are concentration, phase, or polarization that define the composition or structure. Phase-field simulations often utilize thermodynamic and kinetic parameters as input constants.

An initial microstructure can be generated by assuming small randomly perturbed values of order parameters at each grid point. The energetically driving force for microstructural evolution is calculated and evaluated in the evolution equation to obtain the final microstructure. The evolution occurs according to the Cahn-Hilliard [58] nonlinear

diffusion equation and the Allen-Cahn [59] (time-dependent Ginzburg-Landau) equation:

$$\frac{\partial \eta_p(\vec{r},t)}{\partial t} = -L_{pq}\frac{\delta F}{\delta \eta_q(\vec{r},t)} \tag{2.1}$$

$$\frac{\partial c(\vec{r},t)}{\partial t} = M\nabla^2\frac{\delta F}{\delta c(\vec{r},t)} \tag{2.2}$$

where r is the position vector, t is time, L_{pq} is the mobility of the non-conserved variables, M is diffusivities of the species, c is the conserved field variable, η_i are the non-conserved field variables, and F is the total free energy of the system. The total energy should take into account both local and long-range interaction energies. The description of the system comes in from the definition of the free energy functional, which in its most basic form takes into account the chemical energy, phase gradient energy, and composition gradient energy.

$$F(f,c,\eta) = \int_V \left[f(c,\eta) + \frac{\kappa_c}{2}(\nabla c)^2 + \frac{\kappa_\eta}{2}(\nabla \eta)^2 dv \right] \tag{2.3}$$

where κ_c and κ_η are the composition and phase gradient energy coefficients, respectively.

Phase-field has become attractive for its use in studying the evolution in solidification [60], spinodal decomposition [61], Martensitic phase transformations [43], grain growth [44], and ferroelectric domain switching [62]. It has been extended multiple times over the past couple of decades to study the effect of strain on domain structure in ferroelectric thin films, as well as the combined effects of interfacial dislocations on phase stability [45].

As described later in greater detail, the evolution of phase-field has tightly followed its applications and derivations for unique material surfaces. The chemical energy, phase-gradient, and composition gradient energies are local energetics, which take into account short range interactions with their neighbors. Further introducing long-range terms in the form of global elastic energy and electrostatic energy, results in new long-range interactions. Phase-field has experienced great success and growth to many areas working with the evolution of ferroelectric domains. Early on, L.Q. Chen used the continuum phase-field

model to simulate grain growth [63]. The effect of thin films was explored by Y.L. Li [64]. It was then expanded to polycrystalline work by Choudhury [65]. Further refinement was performed by Zhang and Bhattacharya on domain models [66, 67] and Su and Landis in 2007[46]. In a recent effort to address a major limiting concern in phase-field, Völker et. al determined phase-field constants from *ab initio* density functional theory [68]. As a result, we will explore the use of phase-field as a basis for data generation to train our machine learning model.

Chapter 3: Methods

3.1 Phase Field Data Generation

The numerical solution of the spatial and temporal evolution of the $PbTiO_3$ ferro-electric domain structure was determined via the time-dependent Landau-Ginzburg-Devonshire equations [69]. The relevant Landau-Ginzburg-Devonshire equations are as follows:

$$\frac{\partial P_i(\boldsymbol{x},t)}{\partial t} = -L\frac{\delta F}{\delta P_i(\boldsymbol{x},t)}, (i = 1,2,3) \tag{3.1}$$

where $\boldsymbol{P}$ represents the vector of ferroelectric polarization, $\boldsymbol{x}$ is the position vector, L is a kinetic coefficient related to the domain mobility, t is time, and F is the total free energy. The total free energy is described by:

$$F = \int_V \left(f_{\text{bulk}} + f_{\text{elas}} + f_{\text{grad}} + f_{\text{elec}}\right) \mathrm{d}V \tag{3.2}$$

where $f_{\text{bulk}}(P_i)$ represents the Landau-Ginzburg-Devonshire uniform unstrained bulk energy, $f_{\text{elas}}(P_i, \epsilon_{kl})$ is the elastic energy density, $f_{\text{grad}}(\nabla P_i)$ is the gradient energy density, and $f_{\text{elec}}(P_i, E_i)$ is the electrostatic energy density, over the volume V. The bulk free energy density is expanded in terms of the local polarization [65]:

$$\begin{aligned} f_{\text{bulk}} = {} & \alpha_1\left[(P_x^L)^2 + (P_y^L)^2 + (P_z^L)^2\right] + \alpha_{11}\left[(P_x^L)^4 + (P_y^L)^4 + (P_z^L)^4\right] + \\ & \alpha_{111}\left[(P_x^L)^6 + (P_y^L)^6 + (P_z^L)^6\right] + \\ & \alpha_{12}\left[(P_x^L P_y^L)^2 + (P_y^L P_z^L)^2 + (P_z^L P_x^L)^2\right] + \\ & \alpha_{112}\left[(P_x^L)^2\left((P_y^L)^4 + (P_z^L)^4\right) + (P_y^L)^2\left((P_z^L)^4 + (P_x^L)^4\right) + (P_z^L)^2\left((P_x^L)^4 + (P_y^L)^4\right)\right] \\ & \alpha_{123}(P_x^L P_y^L P_z^L)^2 \end{aligned} \tag{3.3}$$

where α_1, α_{11}, α_{111}, α_{12}, α_{112}, α_{123} are the dielectric stiffness and higher-order stiffness coefficients under stress-free boundary conditions, and P_x^L, P_y^L, P_z^L are the polarization components local to each grain's orientation.

Further details of the expressions for the energy density relations are expanded in ref [65]. A periodic boundary condition along x and y was applied to Equation 3.1 with a semi-implicit spectral method [41, 65]. The system was represented as a discrete grid of $512l_0 \times 512l_0 \times 1l_0$ points where the grid spacing factor l_0 was 1.0 nm. A forward time step is taken to be $\Delta t/t_0 = 0.05$. The Landau energy coefficients and the electrostrictive coefficients for $PbTiO_3$ are found in refs [64, 70]. The two variables considered were: 1) the grain boundary transition temperature and 2) the maximum misorientation between grains. The grain structure was assumed to be static and does not change with time. The orientation of each grain was assigned randomly at the beginning of each phase-field simulation. For the bicrystalline setup, there was one grain structure with a line dividing them evenly. For the polycrystalline results, the grain structure was kept fixed with 20 grains in a discrete space of 512×512 nm.

The grain boundary transition temperature was chosen to match the experimentally observed paraelectric secondary phases that appear at the grain boundary [71]. We would like to mimic this observed behavior by controlling the phase at the grain boundary. The system of interest is $PbTiO_3$, which experiences a phase transition at 479 °C. Above this temperature the system is paraelectric and does not experience the spontaneous polarization observed in ferroelectrics. However, below this temperature the system becomes ferroelectric. We can artificially change the temperature this phase change occurs at to mimic how paraelectric phases form at the grain boundary. The lower our artificially controlled grain boundary transition temperature is set, the more material at the grain boundary becomes paraelectric.

The angles of each grain are initialized between 0° and 45° for the grain structure and stored. It is assumed that the grain structure is static, and does not evolve with time.

Two coordinate systems were used internally to describe the ferroelectric polarization. A rotated local coordinate system describes the polarization within each grain, as well as a global coordinate system to solve the elasticity and electrostatic equations. Beginning from a paraelectric state with zero applied electric field, each grain structure is initialized for 32,000 iterations. This initialized structure is used for the microstructure analysis and prediction training. To determine the coercive field, a static electric field is further applied incrementally 10,000 iterations to generate a total of 100 points. The coercive field is calculated as $E_c = \left(E_c^+ - E_c^-\right)/2$, where E_c^+ and E_c^- are the positive and negative linear interpolations at zero polarization.

A total of 2048 microstructures were simulated from phase-field to build the testing and training sets for the encoder-decoder model. Each microstructure represented a unique set of processing conditions, as a pair of randomly selected grain boundary transition temperature and grain boundary angle. The grain boundary transition temperature was chosen in the range 5–479°C. Similarly, the angles of the two domains were chosen such that the orientation between grains was in the range 0° and 90°. Approximately 120,000 CPU hours were needed to simulate the microstructures.

3.2 Encoder-Decoder Architecture.

The network model was written using the open source PyTorch software version 1.0 and python 3.7. The model was loosely based on the principle of a variational autoencoder [72]. However, the implementation of the components were very similar to those outlined by Radford et al [73]. The model is built upon two components, an encoder which learns a transformation from the image to a latent vector z, and a decoder which learns a transformation from the latent vector to a final microstructure of size 512×512 with two channels. The two channels represent the local polarization P_l in the x and y directions, respectively.

The structure of the encoder is a modification to the discriminator provided by Radford

et al. using the loss described by Kingma et al [74]. The primary modifications were the addition of an attention layer and increasing the number of convolution layers to account for the higher input resolution of 512×512 pixels, as well as outputting to a vector with len(z) channels. The encoder consists of an attention layer followed by several two-dimensional convolutional layers with kernel size of 4×4 and stride of 2 pixels with 1 pixel padding. Leaky rectified linear unit activation functions and batch normalization are applied to all layers except the input [75]. The encoder optimizes a mean μ and standard deviation σ vectors that are reparametrized into a latent vector space such that $z = \epsilon\sigma + \mu$, where $\epsilon \sim \mathcal{N}(0, 1)$. The encoder loss was defined using Kullback-Leibler divergence:

$$\text{Loss} = \sum_{n=1}^{N} \sigma_n^2 + \mu_n^2 - \log \sigma_n - 1 \tag{3.4}$$

The decoder had similar modifications to increase the output resolution to the desired 512×512 pixels. A standard mean squared error (MSE) loss function was used to compare the decoder output to the phase-field simulated input:

$$l(x, y) = \text{mean}\left([l_1, \ldots, l_N]\right), \qquad l_n = (x_n - y_n)^2 \tag{3.5}$$

where N is the batch size. The networks were initialized using the Xavier method [76].

Several hyper-parameters were tested. Of note for this work were the encoder loss weighting of 0.01, a batch size of 32, and a learning rate for the RMSProp optimizer of 0.000,1[77]. 16 filters were used for both the encoder and the generator at each layer.

3.3 Predictor Architecture

The hyper-parameters involved include the weight of the encoder loss, the number of filters used, the batch size, and the learning rate for the RMSprop optimizer [77]. The encoder loss was set to 0.01. A base of 8 filters were used for both the encoder and the generator. The batch size was set to 64, though it was determined the results did not

strongly depend on batch size. A learning rate of 0.001 was selected and found to work well.

The network was trained on 1792 out of the 2048 unique phase-field generated domain structures. The training process took roughly four hours to accomplish on a Nvidia 1080 Ti GPU. The training set was split such that 256 domain structures were used as a test set.

Chapter 4: Rapid domain structure predictions with neural networks

Material morphology is a critical part of the materials development process. In recent years, there has been a growing drive to incorporate materials informatics to reduce time-to-market while iteratively expanding the database of material properties through modeling and simulation tools [78–81]. The need for cost-effective design of materials is made evident by the Materials Genome Initiative [82–84], and computational tools such as integrated computational materials engineering (ICME)[85]. Many of these high-throughput computational methods have largely been focused on optimizing materials chemistry [12, 86–88]. However, bulk chemistry alone fails to capture many structural and chemical inhomogeneities present in many materials, also known as microstructure. It is known that many desirable properties such as strength, toughness, ferromagnetic properties, and fatigue resistance are strongly tied to the structural and chemical inhomogeneity within a material known as microstructure [89, 90]. Furthermore, there is a strong desire to realize the link between processing, structure, and properties (PSP links). To this end, further optimization of the materials' mesoscale microstructure is necessary to fully realize optimal performance.

Optimizing microstructure through experimental analysis and design is costly and time-consuming. Microstructures have an inherently stochastic nature such that two microstructures of the same material with equivalent properties will not be identical. Computational microstructure characterization and reconstruction (MCR) improves the material design and optimization process by providing methods to quantitatively represent microstructure with consistent results. Beyond classifying individual components and phases within a material, MCR further enables the reproduction of equivalent microstructures from design variables. Microstructure prediction is useful in the design process to

provide statistics about how the processing methods control the structure. These methods may additionally be used to augment limited datasets. MCR ultimately enables building forward and inverse PSP links to design processing parameters that can lead to a target structure.

Due to the difficulty and cost of building a database, previous MCR studies have used stochastic noise generation processes [35, 37] or very limited regimes of experimental microstructures [36, 56, 57]. These methods do not capture relevant physics (noise generation) or have limited transferability (experimental). This study proposes using an experimentally verified phase-field technique to produce adequate samples for learning as an intermediate step between over-simplified structures and experimental work [62]. Phase-field modeling offers a unique method for generating thousands of realistic microstructures with real-world applications in a matter of days. It has been successfully applied to many areas of materials science, from slip systems to ferroelectric behavior and can provide a range of microstructures with both qualitative and semi-quantitative relationships [69, 71, 91]. Phase-field has already been extensively used to provide insight into the structure-property linkage. Structures generated from phase-field contain realistic co-existing features that account for complex long range interactions. Having experimentally observed features enables trained networks to be more readily leveraged toward material design.

Due to the many features and interactions within the microstructure manifold, characterizing and predicting material microstructure is not a trivial process and often requires expert knowledge [92]. Microstructures are inherently complex and present a challenge due to the difference in scale and appearance of many visual features such as grains, ferroelectric domains, and other defects. Dozens of phenomenological models have been built upon the foundation of such features to correlate changes to properties, such as Hall-Petch equation, the Hollomon law, Landau-Devonshire theory, etc. A single class of ultra-high carbon steels may require over 16,000 visual features to be appropriately classified [36]. When studying multiple features that co-exist and are strongly interacting, there can be

non-linear relationships that make it very difficult to predict how the final microstructure will form. For this reason, studying the relationship between processing conditions and microstructure continues to be a core focus of materials science. Linking a wide range of processing conditions to material structure would enable more rapid material development, and can be accomplished through an effective combination of deep learning and phase-field modeling.

An expansive summary of previous work with MCRs can be found elsewhere [55]. Previous work has focused largely on classifying features in the microstructure using point statistics and local image descriptors in conjunction with support vector machines [56, 93]. These methods typically involve dimension reduction of the feature space to a small set of key characteristics. However, dimension reduction methods often have significant information loss. More recently, methods that have incorporated deep learning by leveraging transfer-learning or deep belief networks have shown great promise [35, 37, 94]. These methods have already yielded success in microstructure characterization, demonstrating the potential within deep learning. However, reconstruction efforts have been limited thus far to reproducing noise generated images. Deep learning is a powerful technology that has grown in many parallel fields of science during recent years due to successes in applications of computer vision problems. Deep learning frameworks are able to rapidly learn and classify many objects with near-human precision in some areas given sufficient training data [35, 36, 56]. In addition to being successful at classification and image segmentation tasks, a type of artificial neural networks called generative models can learn to produce images with qualities specified by an initial set of starting parameters [95]. This is akin to providing the processing conditions and producing the desired microstructure. Two categories of generative models are Generative Adversarial Networks (GAN) and Variational Auto-Encoders (VAE). After some initial testing, Variational Auto-Encoders proved to be the more resilient setup.

Reliably predicting microstructure from design variables is an inherently difficult task.

Modeling microstructure typically requires an algorithm with an intrinsic understanding of the physics to determine a physically sound structure. Variational Auto-encoders would allow a network with sufficient training data to determine the characteristic features of a microstructure and reproduce them across different input parameters independent of any prior knowledge of the physics. This method could be applied to many forms of microstructure.

A prominent type of microstructure is the formation of ferroelectric domains, which is key in the study of ceramic materials. Ferroelectric domains are spatially homogeneous regions of spontaneous electric polarization that form below the ferroelectric phase transition. This useful property allows the material to exhibit very different properties over a narrow range of temperatures. Below the ferroelectric transition temperature, ferroelectric materials can develop a spontaneous electric polarization that can be reveresed with the application of an applied electric field [69]. This occurs through the development of ferroelectric domain structures, separated by domain walls, when a paraelectric phase is cooled. The ability to retain a spontaneous electric polarization in the absence of an applied electric field makes these materials prime candidates for new non-volatile memory technologies. Multiple domains can exist within a single grain, a region with the same crystallographic axis. Developing a fundamental understanding of domains and their response to external electric fields is crucial for many applications of ferroelectrics [48]. Although this study focuses on ferroelectric domains and grain structure as starting points for microstructure discussion, surface and misfit dislocations are other considerations to explore.

Domain wall formation and movement is difficult to study and simulate. However, it is a key characteristic in determining the final material properties. The nature of the domain structure is difficult to estimate analytically. Phenomenological models, while capable of accurately conveying the Curie temperature changes, are only applicable where good potentials are known [96]. An alternative method of using thermodynamic phase-field simulation can provide a reasonably accurate depiction of the domain wall

formation and migration energy [69]. Beyond just simulating microstructure under different conditions, phase-field modeling also provides an assortment of physical properties for each microstructure. This makes phase-field an ideal tool for studying the core processing-structure-property linkages in materials science.

In this work, we employ a high-resolution encoder-decoder VAE to learn how the ferroelectric domain structure changes under different design variables from phase-field simulated images. Further, a second predictor network is developed to quantify a material property from the generated ferroelectric structure. These networks would enable the use of modern optimization schemes by providing a computationally inexpensive model that can be continuously trained [15]. Figure 4.1 demonstrates a potential feedback loop in which deep learning is used to optimize a material property using the microstructure. A phase-field simulation is used to generate the initial microstructure dataset that can be used to train the VAE (red box). This work focuses on the creation and training of the two network models, and the adaptive design feedback loop is not implemented in this work. Using a combined approach with phase-field and deep learning brings about many advantages. Primarily, phase-field allows us to observe near-experimental microstructures with a much lower entry cost. We are able to predict microstructure for lead titanate using the processing conditions given grain boundary transition temperature and misorienation between grains for a bi-crystalline system. Phase-field simulation provides an intelligent starting point for a large data set and can be readily produced on workstations in a reasonably short time frame. A workstation with 32 cores can produce sufficient microstructures of lead titanate under varying grain orientations and grain boundary transition temperatures in a matter of days.

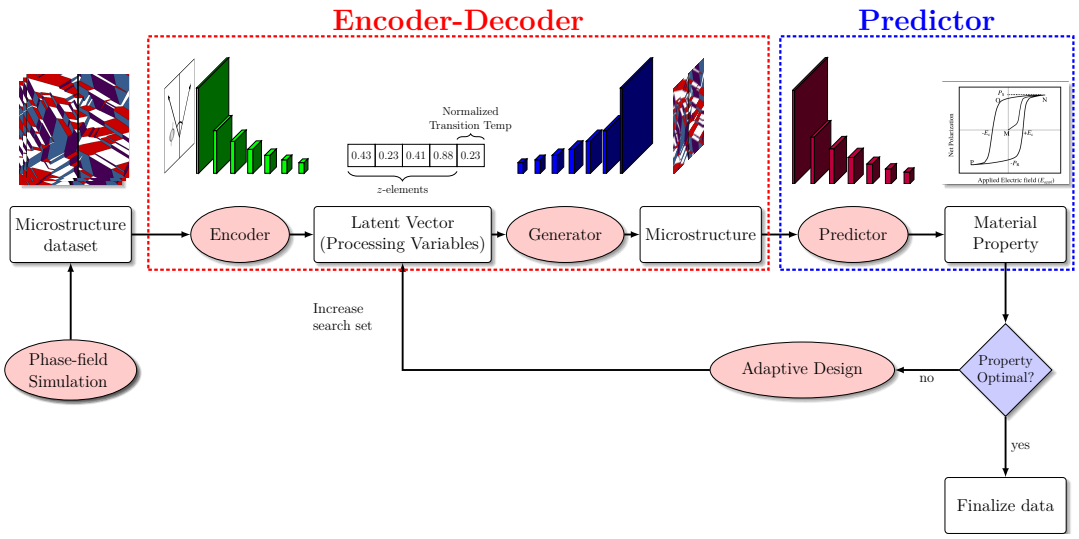

Figure 4.1. Schematic flowchart of the proposed design strategy.

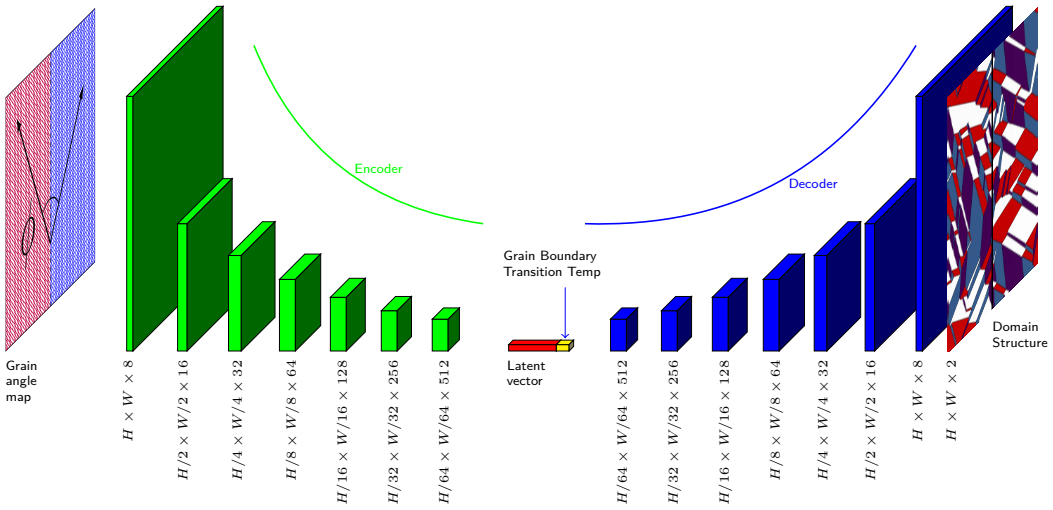

Figure 4.2. Schematic of the encoder-decoder architecture with inputs to each convolutional layer. The encoder-decoder network takes a spatial grain angle map (shown as a bi-crystalline grain in the figure) and produces a lower dimensionality representation in the form of a latent vector. The latent vector is then used in inverse convolutions to produce the ferroelectric domain structure.

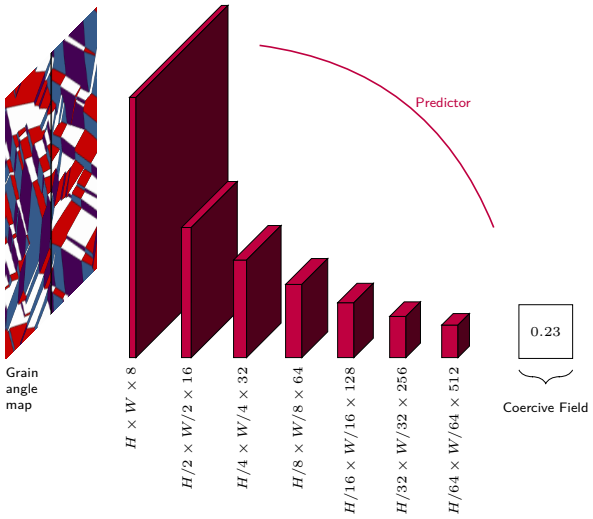

Figure 4.3. Schematic for predictor network that calculates the coercive field based on microstructure input.

4.1 Results and Discussion

4.1.1 Microstructure prediction

To establish the first linkage between processing and microstructure, an encoder-decoder style convolutional neural network (CNN) was used to predict the domain structure given a set of input processing conditions. The ferroelectric domains were predicted for a bi-crystalline two-dimensional 512×512 nm tetragonal $PbTiO_3$ using a multilayer encoder-decoder convolutional neural network. The reference domain structures were produced using a phase-field technique to model the domain evolution and switching in a 2D bi-crystalline grain structure [62]. A training set of 1792 images were used to train the network, while a separate testing set of 256 images was used to evaluate its performance. The testing and training sets had non-overlapping input parameters.

Two input parameters were considered that determine the simulated bi-crystalline microstructure. The first input parameter considered was the ferroelectric transition temperature (T_{GB}), which is used to model effects known to occur at the grain boundary

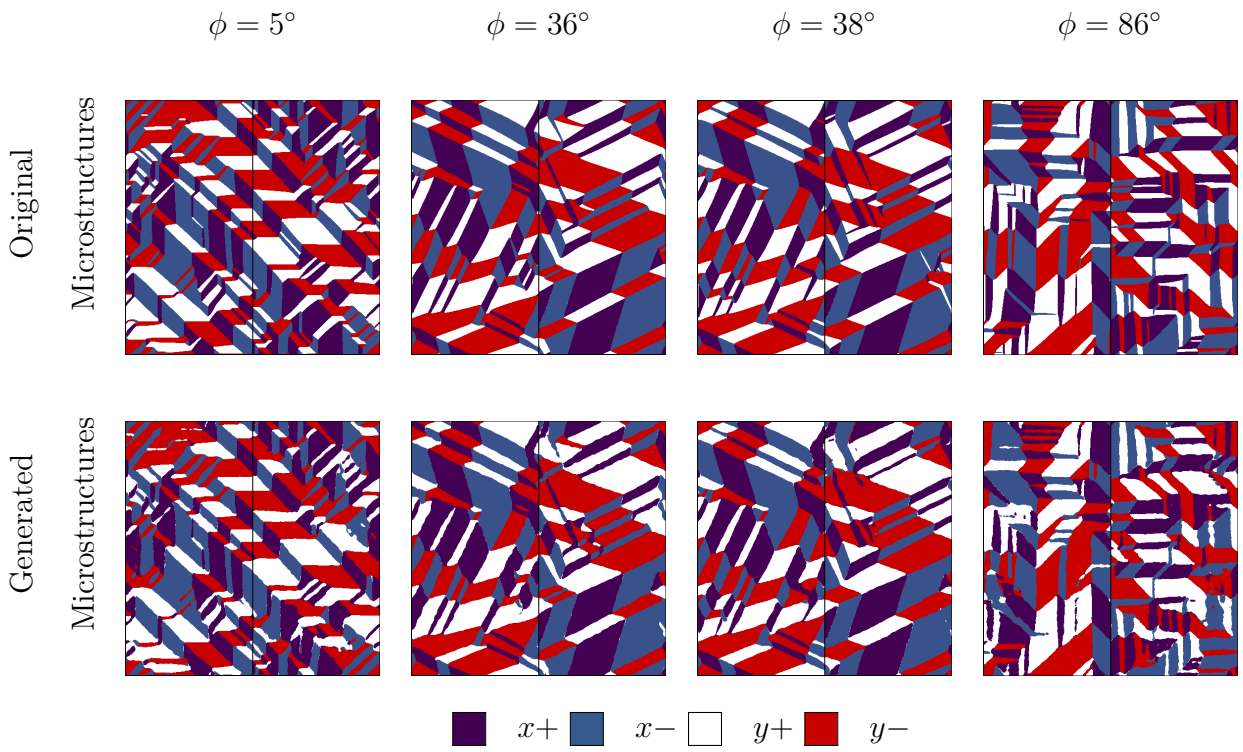

Figure 4.4. Example of training microstructures and microstructures predicted by the network with $T_{GB} = 10\,°\mathrm{C}$.

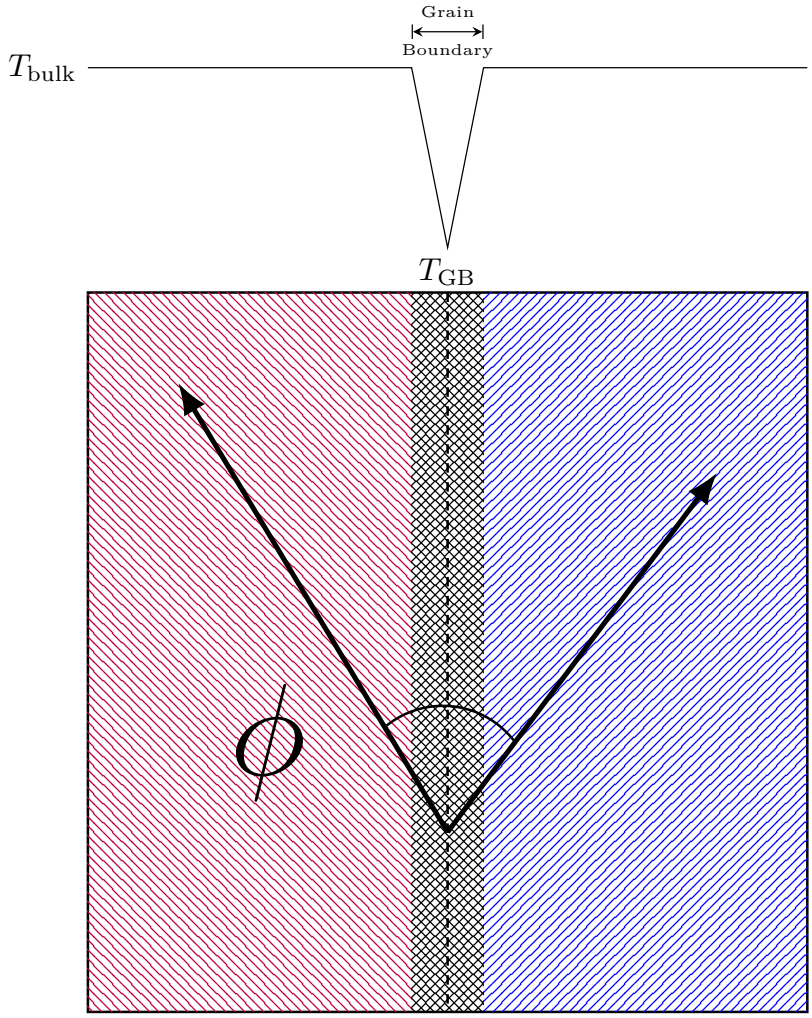

Figure 4.5. Schematic diagram of linear change in transition temperature across a grain boundary.

as a result of processing conditions. For example, lower transitions temperatures simulate the presence of a secondary paraelectric phase that can occur at the grain boundary. This may lead to reduced or zero polarization at the grain boundary. It has been previously shown that the presence of a non-ferroelectric grain boundary layer decreases the dielectric properties in barium titanate ceramics [71]. In this study the grain boundary occurs over a very finite distance of $2\Delta x$, where the transition temperature was changed in a linear fashion as can be seen in Figure 4.5. The transition temperature at the grain boundary was

decreased from 479 °C to 25 °C, which accounted for a significantly increased coercive field. The second considered parameter was the orientation difference between the two grains. has been found to affect the performance of ferroelectric properties. The preferred grain orientation is known to affect polarization switching and influence the overall evolution of ferroelectric domains [62].

Figure 4.4 demonstrates the capabilities of the encoder-decoder to predict domain structures similar to that produced by phase-field over a wide range of input conditions. In tetragonal $PbTiO_3$, the spontaneous polarization can occur in the positive or negative direction of the x and y axis, leading to four possibilities in 2D each of which are equally probable. The ferroelectric domains, regions of similar polarization alignment, are labeled as the $x+$, $y+$, $x-$, and $y-$. The four variants are distinguished with separate shading. In tetragonal, there are two types of domain walls possible to form. In Figure 4.4, a $x+$ domain changing to a $y+$ is separated by a 90° domain wall. Similarly, a 180° polarization is possible.

The resemblances between the domain structure predicted by the encoder-decoder and by phase-field are readily apparent. The encoder-decoder is able to capture and reproduce the changing shape of the domains within the two grains. Further, the encoder-decoder produces similar important physical attributes. For example, a defining attribute observed in phase-field models is the orientation of the ferroelectric domain walls. It is well-known that ferroelectric domains will form such that their edges will be orientated along specific directions dependent on the local angle of the grain [97]. Figure 4.6 compares the measured error of the domain wall angle with the expected domain wall angle due to the orientation of the grain within the 256 sample test set. Each domain wall angle is measured and compared to the expected angle resulting in a total error in degrees. The plot reveals that the encoder-decoder produced microstructures compare favorably to the phase-field produced structures. Due to the nature of imperfect domains, there is an inherent small error in measuring the domain wall angles with line finding algorithms and

also a component of error in the phase-field simulation itself. The phase-field produced microstructures have a built-in average error of 0.84°, demonstrating that there is minimal measurement error. The predictor model performs at an average prediction error of 2.23°.

Figure 4.7 captures the ferroelectric polarization at the grain boundary with differing grain boundary transition temperatures. Along with direction and formation of domains in Figure 4.4, the magnitude of the polarization is also important in several key areas. It has previously been shown that there is a linear trend of increasing polarization magnitude with an increase in transition temperature at the grain boundary [62]. The same behavior is expected to be observed in the encoder-decoder model. The encoder-decoder is able to replicate this linear behavior as this condition is changed.

As can be seen, many of the fundamental physics of the ferroelectric domain features were successfully reproduced by the encoder-decoder. The volume fraction of domain types and the direction of polarization across a high angle grain boundary were also found to be consistent with phase-field. These early results demonstrate the strength of using the presented encoder-decoder scheme as a general tool to predict and generate material microstructure for unique input parameters.

4.1.2 Coercive field Prediction

Beyond providing an effective model to the processing-structure relationship, deep learning can provide insight into the structure-property relationship creating a full processing-structure-property linkage. Phase-field lends itself well to this task, as it can generate many desirable engineering properties of materials beyond just the evolution of microstructures. These simulated properties, such as coercive field, are used to train a model. The coercive field relates the ease at which a ferroelectric will switch polarization directions. It has been shown to be heavily influenced by grain orientations, ferroelectric properties at the grain boundaries [98]. Two important factors in determining coercive field, the ferroelectric transition temperature at the grain boundary and the misorientation between

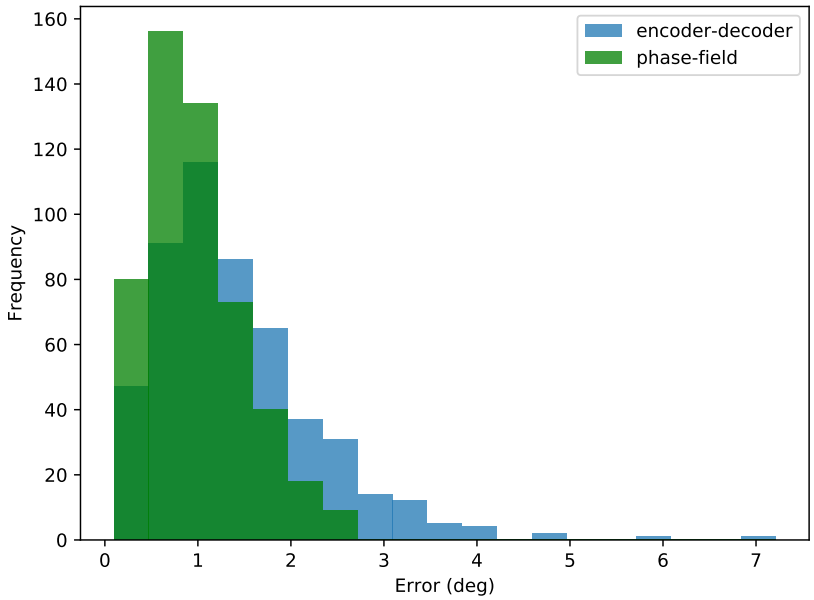

Figure 4.6. Average error represented as angle difference between the actual input grain and the output domain wall orientations. The results from the baseline phase-field are in green with the encoder-decoder model in blue. As seen, the encoder-decoder is showing mildly higher error than the phase-field generated microstructures.

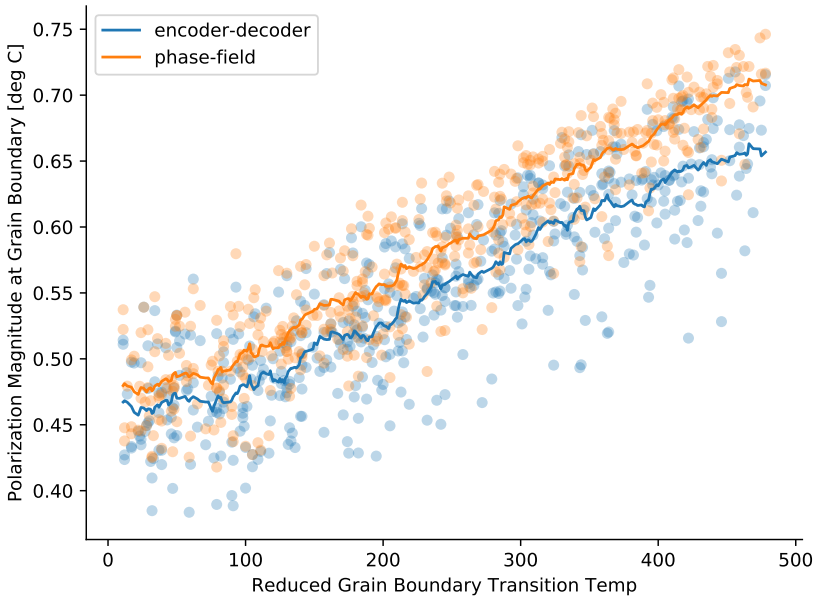

Figure 4.7. Polarization magnitude at the grain boundary as a function of the grain boundary transition temperature. Several data points can be seen for each transition temperature, this difference originates from different grain misorientations for the same transition temperature.

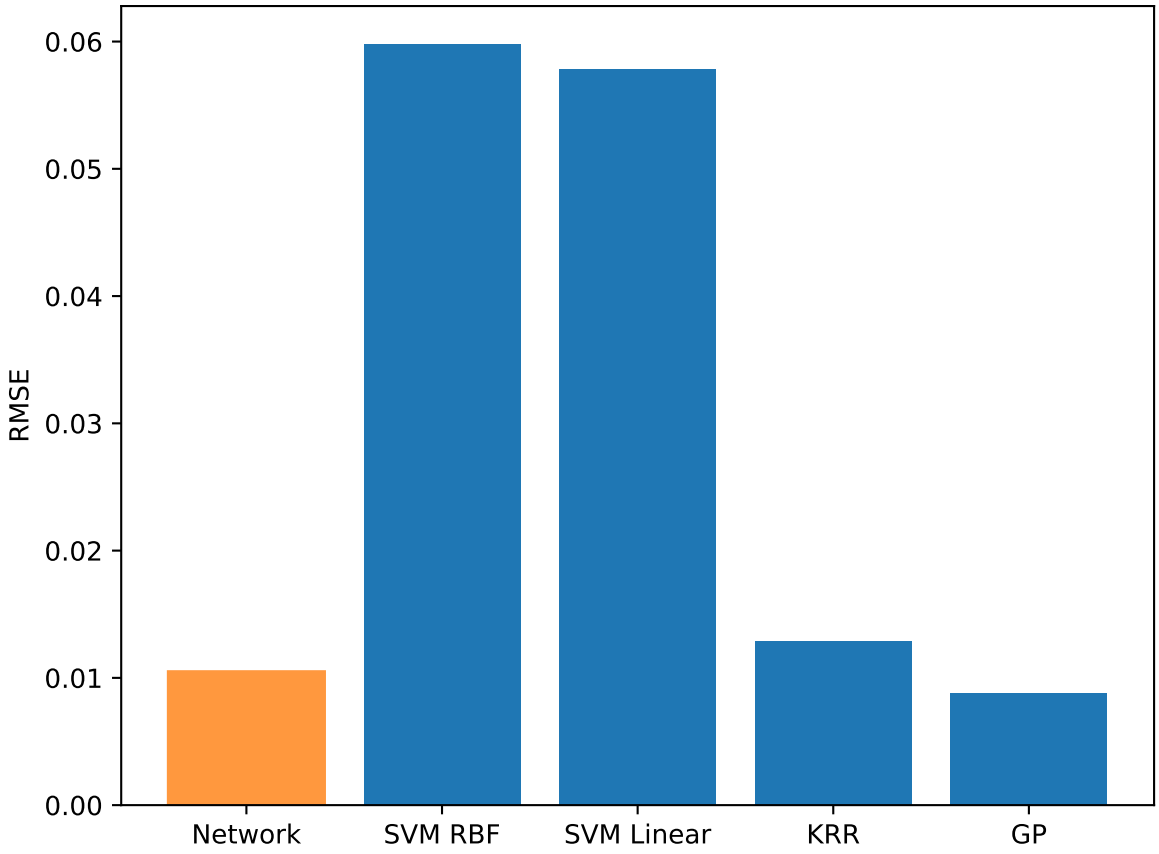

Figure 4.8. RMSE of different machine learning techniques to predict the coercive field. The orange figure is the predictor network presented in this work and takes only microstructure as input. The blue methods were trained using the input processing parameters.

the two grains, have been taken into account to determine the final property through a hysteresis loop in phase-field calculations. Phase-field calculations modeled the evolution of the domains as an applied electric field was applied and reversed.

An independent predictor network was trained to predict the coercive field, given the domain structure of the material. The predictor trained on 1972 domain structures in a similar manner to the encoder-decoder model. Learning the coercive field from the initial domain structure is possible as the coercive field should be a direct result from the formation and arrangement of initial domains. As seen in Figure 4.8, the predictor performs favorably in its property prediction when compared to the phase-field determined

coercive-field.

Figure 4.8 details the ability of common machine learning methods to predict the coercive field of $PbTiO_3$ when supplied with only the grain boundary transition temperature and grain angle. The leftmost column in the figure depicts the results of the predictor which was supplied with only the microstructure. The remaining bars were off-the-shelf machine learning methods that were provided the grain boundary transition temperature and the misorienation between grains as inputs but not the microstructure. The root mean squared error (RMSE) is a common method for determining error of a real-valued prediction. The Gaussian Process (GP), the Kernel Ridge Regression(KRR), and the Linear Support Vector Machine (SVM) had, respectively, an RMSE of 0.0088, 0.0129, 0.0578. With an RMSE of 0.0105, the predictor does better than all except GP, indicating that the predictor can extract the same information from just the microstructure alone.

An encoder-decoder and predictor network were trained which represent the ability of deep neural networks to encapsulate and reproduce the physics of ferroelectric $PbTiO_3$. Together, these networks are able to predict the domain evolution and formation given the processing conditions and then predict the final coercive field property from that microstructure. As demonstrated in Figure 4.1, the two networks jointly can form a regression algorithm that can predict properties, while providing useful visual predictions of the microstructure. This is fundamental in developing understanding of why new materials will be successful. One of the key aspects of materials science is the analysis of microstructural changes in response to a processing change. This relates the physical status of the material to the properties in a visual and useful manner. The patterns and features in microstructure together culminate to detail the processing conditions in a way that simple summary statistics cannot. It is possible to observe a gradient in the ferroelectric transition temperature as a result of composition shift or temperature shift. This will be reflected in the microstructure, but not in summarized processing conditions.

In this study, the random seed used to initialize the phase-field model was kept constant

across all simulations to verify the learning process.

The trained VAE is able to reproduce the polarization directions similar to that predicted by the phase-field code, despite having not seen the combination of properties previously. This is one of the key advantages in deep learning, the ability to automatically learn correlations and reproduce statistically accurate physics without having any explicit domain knowledge programmed in. A cursory visual inspection reveals the encoder-decoder has learned some of the more important aspects of domain formation in $PbTiO_3$. The encoder-decoder was trained using a naive image based L_2 loss function, but was able to capture much of the underlying physics as well, namely the domain wall orientation and the polarization magnitude at the grain boundary.

As noted previously, the orientation of the domain wall angles can be determined analytically and only form along planes with mechanical compatibility [97]. It is known that for 90° domain walls, a grain with 0° orientation the domain wall will form along [1 1 0]. Rotation of the grain will also lead to rotation of the domain wall. Without explicit coding of the loss function to take into account the domain wall formation energies, the network was able to determine the domain wall angle relative to the grains. A quantitative estimate of success can be seen in Figure 4.6. The network predicted domain structures deviated significantly more from the analytically expected domain wall angles than the phase-field model. However, the network is still able to capture this information and only produce an average error of 1.39° higher than that predicted by phase-field modeling. This is only slightly higher than the noise level of the measurement method, as indicated by the error in the phase-field measurements. This achievement indicates that with further addition of phase-field thermodynamics into the network architecture, there will be an even greater success.

4.1.3 Coercive field predictions

The network prediction of coercive field performs better than those predicted by traditional machine learning on the processing conditions alone. This could indicate that the processing conditions were not sufficient to describe the final property outcome. However, the microstructure observed contained more latent information about the final properties and the network was able to predict more accurately. The success of the network is partially dependent on the network being able to capture and analyze long range parameters, such as the domain size, the presence of 180° domain walls, and more. Such interactions may form a more complete depiction of the total system than processing conditions alone.

Chapter 5: Applying generalized method to polycrystalline systems

5.1 Introduction

Recently, there has been considerable interest in investigating and improving low cost poly-crystalline piezoelectric devices [54, 99–103]. Lead zirconate titanate (PZT) and barium titanate $BaTiO_3$ are typical piezoelectric materials found in industry thanks to their combination of large piezoelectric constants, temperature stability, and the cost efficiency of polycrystalline ceramics. Recent studies have shown that domain structures of PZT contains both short-range and long-range organization of ferroelectric domains. It can be seen that domains need to minimize energy in short-range with their orientation respect to their immediate neighbors, causing narrow stripes in opposing directions to form. However, across many defects such as grain boundaries or interfaces, these form much more important interactions. The organization of these narrow stripe regions now effects the macroscopic properties we observe and care about. The phase-field model takes into account both long-range and short-range interactions and can be distinguished between each other. This makes phase-field modeling and ideal tool to probe into these interactions and their effect on properties. Low cost devices are dependent upon polycrystalline processing. Identifying the sources that lead to a particular microstructure can lead to ultimately understanding how to improve properties exhibited by polycrystalline microstructure.

In order to understand how microstructure is developed energetically, we must first have a general knowledge of what microstructure contains. Typically we think of microstructure as a collection of extrinsic strains from atomic defects, dislocations, interfaces, etc. The presence of strains can immediately effect the rotation of polarization. This has a long-range effect which ultimately degrades properties due to pinning domain walls and suppressing

switching. Furthermore, it has been observed that piezoelectric properties change spatially depending on input grain structure and strain [104]. Together, this demonstrates that there is a need for understanding what the source of these long-range and short-range interactions are and how we can distinguish them. Many machine learning techniques, such as neural networks may be applied to this extent.

Artificial neural networks have been increasingly applied to improve performance and automate tasks in materials science with respect to microstructure [35, 37, 57]. A series of rapid advances since 2012 have enabled networks to automate many tasks, including defect analysis in electron microscopy [105], classification and segregation of steels [106], and analyze ferroelectric performance [**curtis_2019**]. Such tasks involve the microstructure which has historically been difficult to model due to the complex long-range relationships and built-in entropy. Neural networks have become prevalent in many science disciplines due to their versatility, but are still in their infancy and the applications are just beginning to be understood. However, they introduce a powerful new tool in unlocking modeling applications directly on the materials microstructure rather than summary heuristics. Microstructure-sensitive design is key in controlling reaction rate, charge transport, and other features critical to modern applications.

Current methods in microstructure characterization and reconstruction (MCR) are incapable of taking design variables, such the processing conditions, into consideration when reconstructing a microstructure. Building a model capable of taking a wide range of design variables would be desirable to compare the effect of many combinations of design variables without expensive simulation or experimentation. Furthermore, spatial design variables should be considered, such as the effect of specific grain shape or sizes. This is a much more complex development that requires the input to be characterized and encoded before a final microstructure is produced. A model that can accurately predict microstructure based on a set of spatial design variables would enable faster exploration and thus more rapid material development.

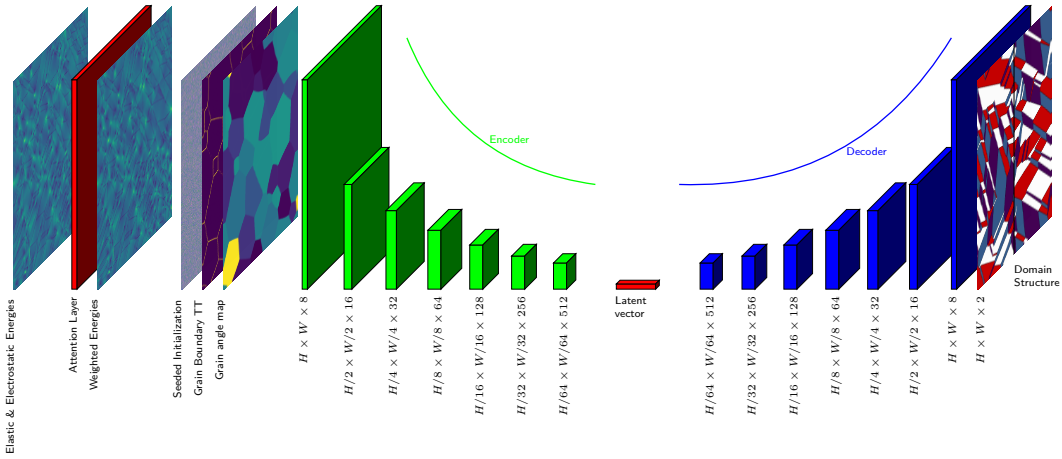

Figure 5.1. Schematic flowchart of the Micro-Attention Net, the proposed design to capture and differentiate the affect of multiple inputs on the final microstructure.

This work aims to create a flexible model, the Micro-Attention Net (MAN) to map spatial design variables to a polycrystalline microstructure using modern machine learning approaches. Furthermore, this work demonstrates that such a model can infer useful context about the generated microstructure, such as the importance each energy input has on the produced structure. In this work we observe two contributions to the ferro-electric microstructure: the elastic energy and the electro-static energy. Developing understanding of how different design variables contribute to the final microstructure product is crucial to microstructure design.

Figure 5.1 demonstrates the MAN model. The input is six different channels, two are the randomly initialized starting points, two channels are maps of the elastic and electrostatic energies. The remaining two channels are the grain boundary transition temperature, and the map of the original grain structure. The two energy channels are fed into an attention layer, which determines the weight of the channels for later, and then concatenated with the remaining four channels, which are then together passed into an encoder, resulting in a small latent vector that describes the input in a compressed form. The latent vector is then applied in the generator, which consecutively up-scales the result into the final microstructure.

5.2 Methods

The same method was applied from chapter 3 with some additions to the network. An attention network was added to the beginning of the network. This attention network used a series of convolutional and pooling layers to down sample the image, then followed with multiple transpose convolutions building a "U" shaped architecture. This method has been shown to be effective in other research areas [107].

This work extended previous work by accounting for energetics in addition to the selected design variables. Previous works relied on a spatial input of the grain boundaries, grain boundary transition temperature, and the orientation of each grain. This work relies on the energetics produced by phase-field calculation as sole inputs. Two energetics were considered, the elastic energy and the electrostatic energy. These were taken directly from the intermediate steps in a phase-field calculation.

5.3 Results & Discussion

To build new understanding of the process-microstructure linkage and of the contributing energetic factors, an encoder-decoder convolutional neural network was designed to predict the formation of microstructure under different design variables. This implementation is the Micro-Attention Net (MAN). To demonstrate the utility of the proposed model, the ferroelectric domains were predicted in a typical polycrystalline two-dimensional 512×512 nm tetragonal $PbTiO_3$. The reference microstructures used for training were produced with a semi-implicit phase-field technique to model the temporal domain evolution and switching in a poly-crystalline system [65]. MAN was evaluated on a distinct testing set of 256 images with input design parameters not yet seen previously.

Three design variables were considered, the grain boundary ferroelectric transition temperature, the maximum allowed grain angle, and the grain structure. Limiting the grain angle limits the orientation difference that can occur between grains. Furthermore, the

ferroelectric transition temperature affects how the domains react to the grain boundaries, and can be likened to having the presence of secondary phases at the grain boundary.

Figure 5.2 outlines how design variables can result in different microstructures. The top row contains domain structures directly from phase-field calculation. Each image in the row contains a different set of input design parameters. Despite a static seed, each microstructure is very different than every other microstructure. The second row shows results from the MAN model when given the same inputs as the phase-field simulation and trained on a static seed. The result is a microstructure that looks nearly identical in domain structure to that produced by the phase-field simulation, albeit with the presence of some artifacts. The final row is similar, except the MAN model produces output when trained on randomly seeded data. As expected, the performance is significantly worse. This is due to the randomness built in to microstructures.

A major obstacle preventing easy microstructure analysis is their inherent stochasticity. Despite being prepared with near identical conditions, microstructures will form that are completely distinct from one another. Grain boundaries will not be in the same place, and the number of grains is not guaranteed to be the same. In the case of the second row, this object is removed by fixing the seed to a constant value and every microstructure produced by phase-field will be identical if given identical inputs. Conversely, the third row has been trained with each microstructure taking on a unique seed value. This results in the model having to generalize much of the output. During this operation, many artifacts are produced.

Beyond just looking at the microstructure prediction, another aspect of the network is the addition of a attention layer. An attention layer exists to learn the relative importance of each input. This is useful, for instance, when determining what input contributes most to the microstructure. In Figure 5.3, we can see the output of this attention layer when looking at two input energies: the elastic energy and the electrostatic energy. The figure captures the weight for each microstructure in the test set. As seen in the figure,

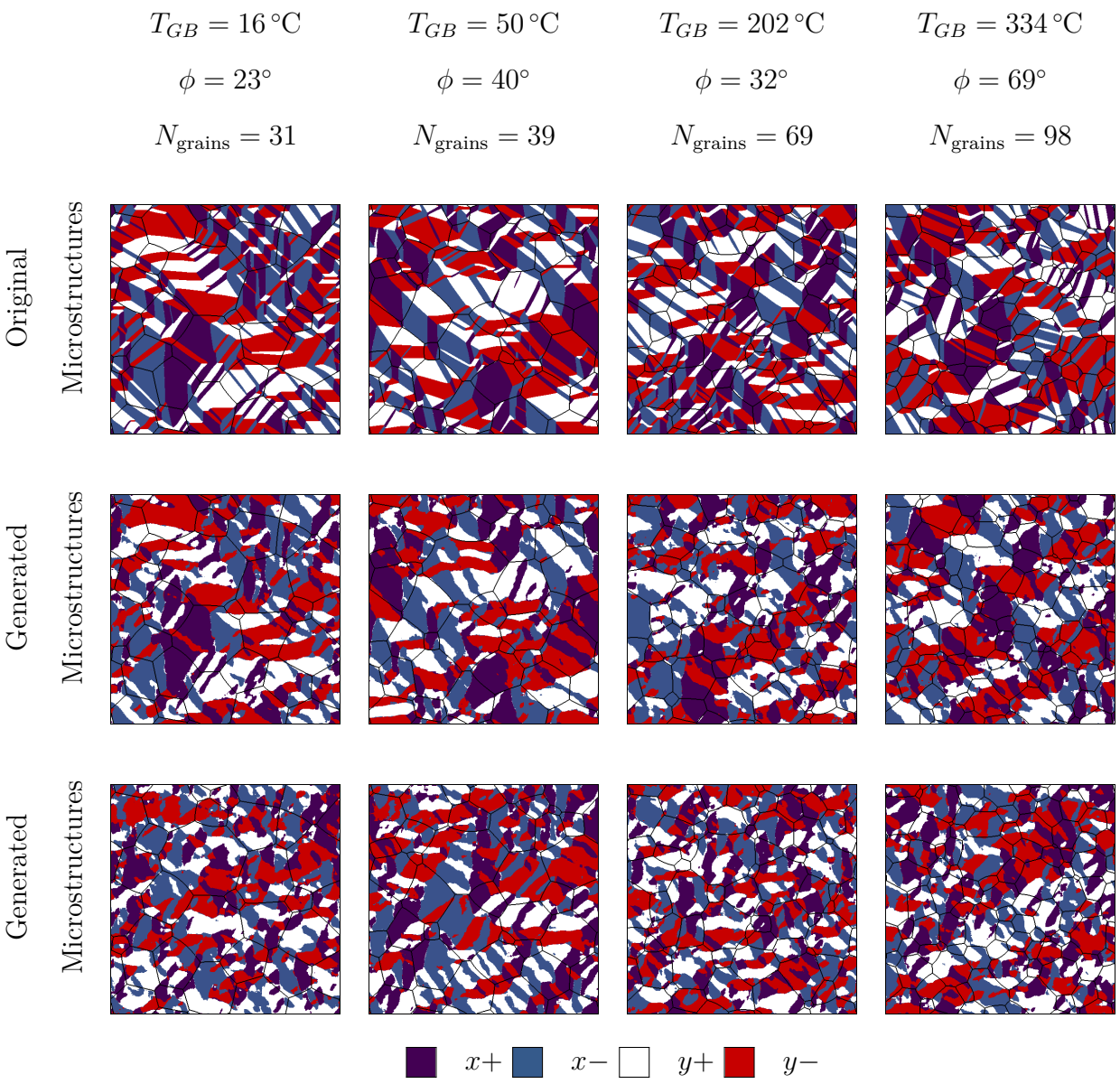

Figure 5.2. Example of testing batch microstructures and microstructures predicted by the encoder-decoder. The middle row contains a seed that was seen during training. Conversely, the bottom row is a new seed not previously encountered.

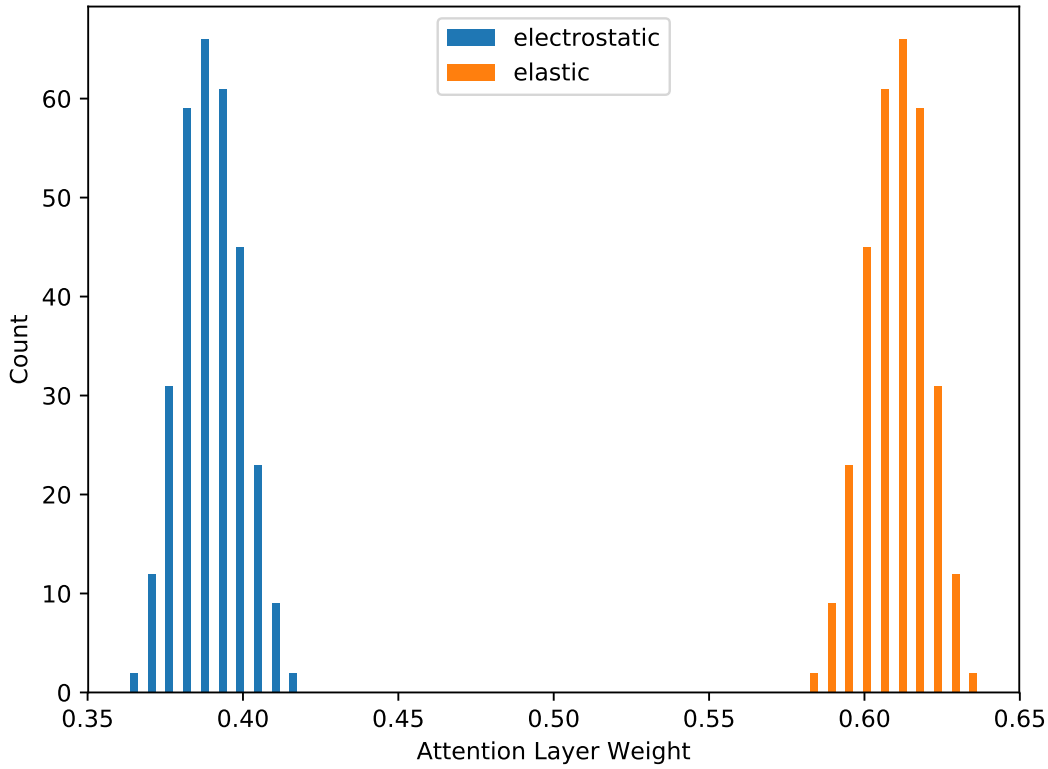

Figure 5.3. Histogram of the attention weights distributed across the testing set. A distinction between the associated weights of electrostatic and the elastic energies can be seen.

a distribution appears centered on 0.4 and 0.6, for the electrostatic and elastic energies, respectively. This indicates that the relative importance of the electrostatic and elastic energies fluctuate from input to input, but not very greatly. Furthermore, Figure 5.3 demonstrates that in this instance, the elastic energy is the dominant contributing factor to the formation of ferroelectric domains in our studied $PbTiO_3$ data set. The electrostatic energy is given less weight, but it is not ignored completely, indicating it too is critical to determine the final microstructure.

5.4 Conclusion

The Micro-Attention Net model was designed and implemented to predict microstructure formation given spatial inputs. Furthermore, an attention model was built into it

that could determine the relative importance of each input type across the microstructure. The MAN model can reasonably reproduce results from a statically generated dataset. However, it is limited in its ability to learn and generalize from a truly random training set. Despite this limitation, it was shown to identify a difference in the relative importance of elastic and electrostatic energies in their bulk contribution to the final domain structure. Furthermore, it was able to present a spatial distribution of the importance of each input. From this, we can see what inputs contributed most to what final microstructure feature. Ultimately, this model shows great promise in its ability to aid in microstructure understanding and design.

5.5 Acknowledgments

This work was supported financially by the generous support of the National Science Foundation Graduate Research Fellowship Program under Grant No. 1842399.

Chapter 6: Summary and Future Work

As mentioned in Chapter 1 the primary objective of this thesis is to develop a general model capable of linking microstructure to both processing conditions and to properties. In particular, to develop a model that could capture many of the complex short-range and long-range interactions within a microstructure and be able to reproduce them in a statistically equivalent image following the principles of Microstructure Characterization and Reconstruction. Microstructure is studied in many aspects of materials science and plays a critical role in the development of new materials. A material microstructure is a direct result of the processing conditions and chemical makeup, but also directly correlates to the final properties a material will have. This relationship, that of the processing-microstructure-property, is ubiquitous throughout materials science. This work ambitiously aims to build a general model that can capture many features of the microstructure, and then predict a new microstructure under various conditions automatically.

To this end, a general model designed using a machine learning approach with Convolutional Neural Networks (CNNs) was developed and tested on bi-crystalline lead-titanate that had been simulated with a phase-field technique. The model successfully predicted ferroelectric domain wall orientation, volume fraction, and grain boundary polarization in bi-crystalline lead-titanate. Further, an extension of the model was shown to successfully estimate the coercive field based on the initial ferro-electric domain structure.

6.1 Limitations

One of the strongly limiting aspects of the current model is the noise apparent in the predictions. Despite that many features (volume fraction of domains, domain orientation, etc.) were successfully predicted and captured, other aspects appear that are non-physical. There are often small regions that are inconsistent with the surrounding area. These "islands" are often a domain direction that is inconsistent with the surrounding domain

and may be entirely encompassed by one domain. Such an area does not physically appear in the simulations. Furthermore, the shape of these defects is incongrous with the overall shape of many domains. The regular domains typically form in straight laminar segments, whereas the defects often appear in circular regions.

6.2 Future Directions

One aspect of neural networks that limits their application is the number of parameters to be trained. Jon von Neumann famously said "With four parameters I can fit an elephant, and with five I can make him wiggle his trunk." The networks trained in this work were on the order of millions of parameters. The sheer number of which drastically increases the computational cost. Even with efficient codebases and using modern GPU calculations, scaling this project to larger image sizes would be nearly impossible to train without reconsidering the network architecture. One interesting direction would be to limit the number of parameters in the network and use external tools to increase the produced image size. Recent work has been progressing rapidly on super-resolution image techniques, which are able to enhance an image resolution.

Taking the scaling argument a little further in a direction important to materials science would be to look at the case of 3D microstructures. While we often look at 2D microstructures, the real information is 3D and we simply take a 2D sample. The technologies used in this thesis already exist in 3D, and even phase-field has long been used on 3D as seen in Figure 6.1. This would require being able to scale the input accordingly, but new efficient 3D convolutions are already working in other fields. 3D microstructures may well drastically improve the results and reveal new features.

This work shows the potential of current convolutional strategies for encoding a spatial input and then predicting a new microstructure from that input. Presently, it requires thousands of labeled samples in order to successfully train. Acquiring a database of experimental samples this large would require a massive collective effort from several

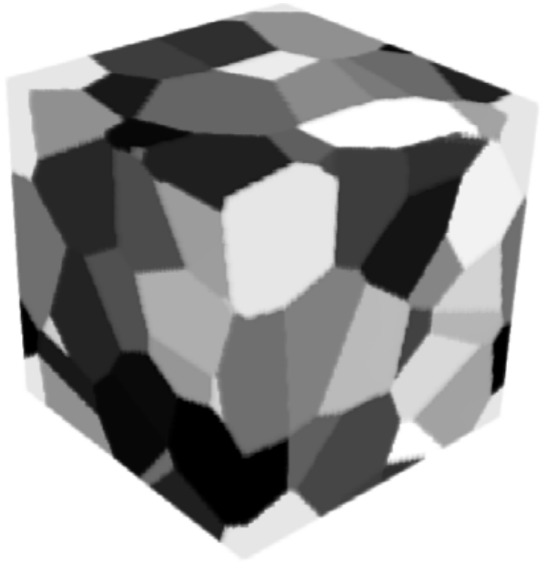

Figure 6.1. An example of three dimensional phase-field output [108].

students and universities. However, there is a current field of study observing transfer learning [109]. It demonstrates that a previously trained model could be used on an entirely new application with little modification. Furthermore, it has been shown that a model may initialize weights from a previously trained model and be successfully applied to a new area with much fewer samples. In this case, it may be possible to train the model with simulation techniques, such as phase-field, and then train on a very small data set consisting of only a couple dozen samples. The model could then be used in tandem with data-driven machine learning techniques to quickly focus on property optimization in a few steps.

While developing and testing on experimental data is the ideal moving target, there are many recent developments that could improve the current state of the model. These new methods may provide greater accuracy and insight while removing key limitations of the current model, such as the island defects. The first is the addition of an adversarial network. An adversarial network severely increases the complexity of training the model, but also does not use a defined loss function. Ideally, this network should reproduce statistically equivalent images. However, the description of statistically equivalent evolves for each

image. Instead, this network is trained on static images and is expected to reproduce them based on an intial state. Adding an adversarial network would remove this requirement and instead the network would be the loss function. It would allow the model to predict truly stochastic microstructures.

Another improvement to the network architecture in addition to adversarial networks could be transferring expert knowledge into the network from phase-field. This would reduce the number of training images needed, and also improve accuracy. One potential implementation would accomplish this by taking energy functionals described in the phase-field model and enforce the network to minimize these as well in its output. This would incorporate much of the knowledge the network needs to learn. This method loses the overall generalization of the project but is expected to bring significant performance and usability improvements. This improvement, along with other listed could bring significantly better accuracy and prediction skills.

References

1. Hall, E. O. The Deformation and Ageing of Mild Steel: III Discussion of Results. *Proc. Phys. Soc. B* **64,** 747. ISSN: 0370-1301. http://stacks.iop.org/0370-1301/64/i=9/a=303 (2018) (1951).

2. Hume-Rothery, W. *Atomic Theory for Students of Metallurgy* 342 pp. (Institute of Metals, 1952).

3. Dreizler, R. M. & Gross, E. K. U. *Density Functional Theory: An Approach to the Quantum Many-Body Problem* 312 pp. ISBN: 978-3-642-86105-5 (Springer Science & Business Media, Dec. 6, 2012).

4. Warren, J. A. & Boettinger, W. J. Prediction of Dendritic Growth and Microsegregation Patterns in a Binary Alloy Using the Phase-Field Method. *Acta Metallurgica et Materialia* **43,** 689–703. ISSN: 0956-7151. http://www.sciencedirect.com/science/article/pii/095671519400285P (2019) (Feb. 1, 1995).

5. Ma, D., Friák, M., von Pezold, J., Raabe, D. & Neugebauer, J. Computationally Efficient and Quantitatively Accurate Multiscale Simulation of Solid-Solution Strengthening by Ab Initio Calculation. *Acta Materialia* **85,** 53–66. ISSN: 13596454. https://linkinghub.elsevier.com/retrieve/pii/S1359645414008088 (2019) (Feb. 2015).

6. Lookman, T. *Information Science for Materials Discovery and Design | Turab Lookman | Springer* //www.springer.com/us/book/9783319238708 (2017) (2016).

7. Rajan, K. Materials Informatics: The Materials Gene and Big Data. *Annual Review of Materials Research* **45,** 153–169 (2015).

8. *Materials Genome Initiative | WWW.MGI.GOV* https://www.mgi.gov/ (2018).

9. Chial, H. DNA Sequencing Technologies Key to the Human Genome Project. *Nature Education* **1,** 219 (2008).

10. Kalidindi, S. R. & De Graef, M. Materials Data Science: Current Status and Future Outlook. *Annu. Rev. Mater. Res.* **45,** 171–193. ISSN: 1531-7331. http://www.annualreviews.org/doi/10.1146/annurev-matsci-070214-020844 (2017) (July 1, 2015).

11. Wall, T. D., Corbett, J. M., Martin, R., Clegg, C. W. & Jackson, P. R. Advanced Manufacturing Technology, Work Design, and Performance: A Change Study. *Journal of Applied Psychology* **75,** 691–697. ISSN: 1939-1854, 0021-9010. http://doi.apa.org/getdoi.cfm?doi=10.1037/0021-9010.75.6.691 (2018) (1990).

12. Jain, A. *et al.* Commentary: The Materials Project: A Materials Genome Approach to Accelerating Materials Innovation. *APL Materials* **1,** 011002. http://aip.scitation.org/doi/abs/10.1063/1.4812323 (2018) (July 1, 2013).

13. Gossett, E. *et al.* AFLOW-ML: A RESTful API for Machine-Learning Predictions of Materials Properties. *Computational Materials Science* **152,** 134–145. ISSN: 0927-0256. http://www.sciencedirect.com/science/article/pii/S0927025618302349 (2019) (Sept. 1, 2018).

14. Trump, D. *Executive Order on Maintaining American Leadership in Artificial Intelligence* https://www.whitehouse.gov/presidential-actions/executive-order-maintaining-american-leadership-artificial-intelligence/ (2019).

15. Balachandran, P. V., Xue, D., Theiler, J., Hogden, J. & Lookman, T. Adaptive Strategies for Materials Design Using Uncertainties. *Sci Rep.* **6.** ISSN: 2045-2322. pmid: 26792532. https://www.ncbi.nlm.nih.gov/pmc/articles/PMC4726355/ (2017) (Jan. 21, 2016).

16. Jones, D. R., Schonlau, M. & Welch, W. J. Efficient Global Optimization of Expensive Black-Box Functions. *Journal of Global Optimization* **13,** 455–492. ISSN: 0925-5001, 1573-2916. https://link.springer.com/article/10.1023/A:1008306431147 (2017) (Dec. 1, 1998).

17. Ziegler, G., Heinrich, J. & Wötting, G. Relationships between Processing, Microstructure and Properties of Dense and Reaction-Bonded Silicon Nitride. *J Mater Sci* **22,** 3041–3086. ISSN: 0022-2461, 1573-4803. https://link.springer.com/article/10.1007/BF01161167 (2018) (Sept. 1, 1987).

18. Samuel, A. L. Some Studies in Machine Learning Using the Game of Checkers. *IBM Journal of Research and Development* **3,** 210–229. ISSN: 0018-8646 (July 1959).

19. Mount, D. W. & Mount, D. W. *Bioinformatics: Sequence and Genome Analysis* (Cold spring harbor laboratory press New York: 2001).

20. Gentleman, R. C. *et al.* Bioconductor: Open Software Development for Computational Biology and Bioinformatics. *Genome Biology* **5,** R80. ISSN: 1474-760X. https://doi.org/10.1186/gb-2004-5-10-r80 (2019) (Sept. 15, 2004).

21. Baldi, P., Baldi, P. P., Brunak, S. & Bach, F. *Bioinformatics: The Machine Learning Approach* 492 pp. ISBN: 978-0-262-02506-5 (MIT Press, 2001).

22. Huang, D. W., Sherman, B. T. & Lempicki, R. A. Bioinformatics Enrichment Tools: Paths toward the Comprehensive Functional Analysis of Large Gene Lists. *Nucleic Acids Res* **37,** 1–13. ISSN: 0305-1048. https://academic.oup.com/nar/article/37/1/1/1026684 (2019) (Jan. 1, 2009).

23. Akella, L. B. & DeCaprio, D. Cheminformatics Approaches to Analyze Diversity in Compound Screening Libraries. *Current Opinion in Chemical Biology. Molecular Diversity* **14,** 325–330. ISSN: 1367-5931. http://www.sciencedirect.com/science/article/pii/S1367593110000438 (2019) (June 1, 2010).

24. LeCun, Y., Bengio, Y. & Hinton, G. Deep Learning. *Nature* **521,** 436–444. ISSN: 0028-0836, 1476-4687. http://www.nature.com/articles/nature14539 (2018) (May 2015).

25. HKDH, B. Neural Networks in Materials Science. *ISIJ international* **39,** 966–979 (1999).

26. Mannodi-Kanakkithodi, A., Huan, T. D. & Ramprasad, R. Mining Materials Design Rules from Data: The Example of Polymer Dielectrics. *Chem. Mater.* **29,** 9001–9010. ISSN: 0897-4756. http://dx.doi.org/10.1021/acs.chemmater.7b02027 (2018) (Nov. 14, 2017).

27. Velickovic, P. *Complete Collection of My PGF/TikZ Figures* Jan. 7, 2018. https://github.com/PetarV-/TikZ (2018).

28. Goodfellow, I., Bengio, Y. & Courville, A. *Deep Learning* 775 pp. ISBN: 978-0-262-03561-3 (The MIT Press, Cambridge, Massachusetts, 2016).

29. Srivastava, N., Hinton, G., Krizhevsky, A., Sutskever, I. & Salakhutdinov, R. Dropout: A Simple Way to Prevent Neural Networks from Overtting, 30.

30. Hinton, G. E. Rectified Linear Units Improve Restricted Boltzmann Machines Vinod Nair (2010).

31. Krizhevsky, A., Sutskever, I. & Hinton, G. E. ImageNet Classification with Deep Convolutional Neural Networks. *Communications of the ACM* **60,** 84–90. ISSN: 00010782. http://dl.acm.org/citation.cfm?doid=3098997.3065386 (2019) (May 24, 2017).

32. Simonyan, K. & Zisserman, A. Very Deep Convolutional Networks for Large-Scale Image Recognition. arXiv: 1409.1556 [cs]. http://arxiv.org/abs/1409.1556 (2018) (Sept. 4, 2014).

33. Lecun, Y., Bottou, L., Bengio, Y. & Haffner, P. Gradient-Based Learning Applied to Document Recognition. *Proceedings of the IEEE* **86,** 2278–2324. ISSN: 0018-9219 (Nov. 1998).

34. Chowdhury, A., Kautz, E., Yener, B. & Lewis, D. Image Driven Machine Learning Methods for Microstructure Recognition. *Comput. Mater. Sci.* **123,** 176–187. ISSN: 0927-0256. http://www.sciencedirect.com/science/article/pii/S0927025616302695 (2016) (Oct. 2016).

35. Lubbers, N., Lookman, T. & Barros, K. Inferring Low-Dimensional Microstructure Representations Using Convolutional Neural Networks. *Phys. Rev. E* **96.** ISSN: 2470-0045, 2470-0053. arXiv: 1611.02764. http://arxiv.org/abs/1611.02764 (2017) (Nov. 9, 2017).

36. DeCost, B. L., Francis, T. & Holm, E. A. Exploring the Microstructure Manifold: Image Texture Representations Applied to Ultrahigh Carbon Steel Microstructures. *Acta Materialia* **133,** 30–40. ISSN: 1359-6454. http://www.sciencedirect.com/science/article/pii/S1359645417303919 (2017) (July 2017).

37. Yang, Z. *et al.* Microstructural Materials Design via Deep Adversarial Learning Methodology. arXiv: 1805.02791 [cond-mat, physics:physics]. http://arxiv.org/abs/1805.02791 (2018) (May 7, 2018).

38. Koch, W. & Holthausen, M. C. *A Chemist's Guide to Density Functional Theory* 534 pp. ISBN: 978-3-527-80281-4 (John Wiley & Sons, Nov. 18, 2015).

39. Petrenko, R. & Meller, J. in *Encyclopedia of Life Sciences* (ed John Wiley & Sons, Ltd) (John Wiley & Sons, Ltd, Chichester, UK, Mar. 15, 2010). ISBN: 978-0-470-01617-6 978-0-470-01590-2. http://doi.wiley.com/10.1002/9780470015902.a0003048.pub2 (2019).

40. Botu, V. & Ramprasad, R. Adaptive Machine Learning Framework to Accelerate Ab Initio Molecular Dynamics. *International Journal of Quantum Chemistry* **115,** 1074–1083. ISSN: 1097-461X. https://onlinelibrary.wiley.com/doi/abs/10.1002/qua.24836 (2019) (2015).

41. Chen, L.-Q. Phase-Field Models for Microstructure Evolution. *Annual Review of Materials Research* **32,** 113–140. http://dx.doi.org/10.1146/annurev.matsci.32.112001.132041 (2017) (2002).

42. Boettinger, W. J., Warren, J. A., Beckermann, C. & Karma, A. Phase-Field Simulation of Solidification. *Annual Review of Materials Research* **32,** 163–194. https://doi.org/10.1146/annurev.matsci.32.101901.155803 (2018) (2002).

43. Jin, Y. M., Artemev, A. & Khachaturyan, A. G. Three-Dimensional Phase Field Model of Low-Symmetry Martensitic Transformation in Polycrystal: Simulation of Z2 Martensite in AuCd Alloys. *Acta Materialia* **49,** 2309–2320. ISSN: 1359-6454. http://www.sciencedirect.com/science/article/pii/S1359645401001082 (2018) (July 17, 2001).

44. Krill III, C. E. & Chen, L. .-.-Q. Computer Simulation of 3-D Grain Growth Using a Phase-Field Model. *Acta Materialia* **50,** 3059–3075. ISSN: 1359-6454. http://www.sciencedirect.com/science/article/pii/S1359645402000848 (2018) (July 17, 2002).

45. Hu, S. Y., Li, Y. L. & Chen, L. Q. Effect of Interfacial Dislocations on Ferroelectric Phase Stability and Domain Morphology in a Thin Film a Phase-Field Model. *Journal of Applied Physics* **94,** 2542–2547. ISSN: 0021-8979. http://aip.scitation.org/doi/10.1063/1.1590416 (2018) (July 29, 2003).

46. Su, Y. & Landis, C. M. Continuum Thermodynamics of Ferroelectric Domain Evolution: Theory, Finite Element Implementation, and Application to Domain Wall Pinning. *Journal of the Mechanics and Physics of Solids* **55,** 280–305. ISSN: 0022-5096. http://www.sciencedirect.com/science/article/pii/S0022509606001256 (2019) (Feb. 1, 2007).

47. Li, Y., Hu, S., Sun, X. & Stan, M. A Review: Applications of the Phase Field Method in Predicting Microstructure and Property Evolution of Irradiated Nuclear Materials. *npj Computational Materials* **3.** ISSN: 2057-3960. http://www.nature.com/articles/s41524-017-0018-y (2019) (Dec. 2017).

48. Auciello, O., Scott, J. F. & Ramesh, R. The Physics of Ferroelectric Memories. *Physics Today.* http://physicstoday.scitation.org/doi/10.1063/1.882324 (2018) (July 1998).

49. RABE, K., Ahn, C. & Triscone, J.-M. *Physics of Ferroelectrics: A Modern Perspective* http://archive-ouverte.unige.ch/unige:12885 (2018) (2007).

50. Spaldin, N. A. & Fiebig, M. The Renaissance of Magnetoelectric Multiferroics. *Science* **309,** 391–392. ISSN: 0036-8075, 1095-9203. pmid: 16020720. http://science.sciencemag.org/content/309/5733/391 (2018) (July 15, 2005).

51. Choudhury, S. *Computer Simulations of Ferroelectric Domain Structure and Switching Using Phase-Field Approach* (2008). https://etda.libraries.psu.edu/files/final_submissions/5922 (2018).

52. Choudhury, S., Chen, L. Q. & Li, Y. L. Correlation between Number of Ferroelectric Variants and Coercive Field of Lead Ziconate Titanate Single Crystals. *Appl. Phys. Lett.* **91,** 032902. ISSN: 0003-6951. http://aip.scitation.org/doi/full/10.1063/1.2759274 (2017) (July 16, 2007).

53. Abrahams, S. C. Structurally Based Predictions of Ferroelectricity in Seven Inorganic Materials with Space Group Pba2 and Two Experimental Confirmations. *Acta Cryst B, Acta Cryst Sect B, Acta Crystallogr B, Acta Crystallogr Sect B, Acta Crystallogr Struct Sci, Acta Crystallogr Sect B Struct Sci, Acta Crystallogr B Struct Sci Cryst Eng Mater* **45,** 228–232. ISSN: 0108-7681. //scripts.iucr.org/cgi-bin/paper?st0310 (2018) (June 1, 1989).

54. Ivry, Y., Chu, D., Scott, J. F. & Durkan, C. Domains Beyond the Grain Boundary. *Advanced Functional Materials* **21,** 1827–1832. ISSN: 1616-3028. https://onlinelibrary.wiley.com/doi/abs/10.1002/adfm.201002142 (2018) (May 24, 2011).

55. Bostanabad, R. *et al.* Computational Microstructure Characterization and Reconstruction: Review of the State-of-the-Art Techniques. *Prog. Mater Sci.* **95,** 1–41. ISSN: 0079-6425. http://www.sciencedirect.com/science/article/pii/S0079642518300112 (2018) (June 1, 2018).

56. Azimi, S. M., Britz, D., Engstler, M., Fritz, M. & Mücklich, F. Advanced Steel Microstructural Classification by Deep Learning Methods. *Sci Rep.* **8.** ISSN: 2045-2322. arXiv: 1706.06480. http://arxiv.org/abs/1706.06480 (2018) (Dec. 2018).

57. Kondo, R., Yamakawa, S., Masuoka, Y., Tajima, S. & Asahi, R. Microstructure Recognition Using Convolutional Neural Networks for Prediction of Ionic Conductivity in Ceramics. *Acta Mater.* **141,** 29–38. ISSN: 1359-6454. http://www.sciencedirect.com/science/article/pii/S1359645417307383 (2018) (Dec. 1, 2017).

58. Cahn, J. W. On Spinodal Decomposition. *Acta Metallurgica* **9,** 795–801. ISSN: 0001-6160. http://www.sciencedirect.com/science/article/pii/0001616061901821 (2018) (Sept. 1, 1961).

59. Cahn, J. & Allen, S. A MICROSCOPIC THEORY FOR DOMAIN WALL MOTION AND ITS EXPERIMENTAL VERIFICATION IN Fe-Al ALLOY DOMAIN GROWTH KINETICS. *Journal de Physique Colloques* **38,** C7-51-C7–54. https://hal.archives-ouvertes.fr/jpa-00217210 (2018) (1977).

60. Langer, J. S. in *Directions in Condensed Matter Physics* 0 vols. *Series on Directions in Condensed Matter Physics* Volume 1, 165–186 (WORLD SCIENTIFIC, Aug. 1, 1986). ISBN: 978-9971-978-42-6. http://www.worldscientific.com/doi/abs/10.1142/9789814415309_0005 (2018).

61. Nishimori, H. & Onuki, A. Pattern Formation in Phase-Separating Alloys with Cubic Symmetry. *Phys. Rev. B* **42,** 980–983. https://link.aps.org/doi/10.1103/PhysRevB.42.980 (2018) (July 1, 1990).

62. Choudhury, S., Li, Y. L., Krill, C. & Chen, L. Q. Effect of Grain Orientation and Grain Size on Ferroelectric Domain Switching and Evolution: Phase Field Simulations. *Acta Mater.* **55,** 1415–1426. ISSN: 1359-6454. http://www.sciencedirect.com/science/article/pii/S1359645406007294 (2017) (Feb. 1, 2007).

63. Fan, D. & Chen, L. .-.-Q. Computer Simulation of Grain Growth Using a Continuum Field Model. *Acta Materialia* **45,** 611–622. ISSN: 1359-6454. http://www.sciencedirect.com/science/article/pii/S1359645496002005 (2019) (Feb. 1, 1997).

64. Li, Y. L., Hu, S. Y., Liu, Z. K. & Chen, L. Q. Effect of Substrate Constraint on the Stability and Evolution of Ferroelectric Domain Structures in Thin Films. *Acta Materialia* **50,** 395–411. ISSN: 1359-6454. http://www.sciencedirect.com/science/article/pii/S1359645401003603 (2018) (Jan. 22, 2002).

65. Choudhury, S., Li, Y. L., Krill, C. E. & Chen, L. .-.-Q. Phase-Field Simulation of Polarization Switching and Domain Evolution in Ferroelectric Polycrystals. *Acta Mater.* **53,** 5313–5321. ISSN: 1359-6454. http://www.sciencedirect.com/science/article/pii/S1359645405004672 (2017) (Dec. 1, 2005).

66. Zhang, W. & Bhattacharya, K. A Computational Model of Ferroelectric Domains. Part I: Model Formulation and Domain Switching. *Acta Materialia* **53,** 185–198. ISSN: 1359-6454. http://www.sciencedirect.com/science/article/pii/S1359645404005580 (2019) (Jan. 3, 2005).

67. Zhang, W. & Bhattacharya, K. A Computational Model of Ferroelectric Domains. Part II: Grain Boundaries and Defect Pinning. *Acta Materialia* **53,** 199–209. ISSN: 1359-6454. http://www.sciencedirect.com/science/article/pii/S1359645404005579 (2019) (Jan. 3, 2005).

68. Völker, B., Marton, P., Elsässer, C. & Kamlah, M. Multiscale Modeling for Ferroelectric Materials: A Transition from the Atomic Level to Phase-Field Modeling.

Continuum Mech. Thermodyn. **23,** 435–451. ISSN: 1432-0959. https://doi.org/10.1007/s00161-011-0188-7 (2019) (Sept. 1, 2011).

69. Chen, L.-Q. Phase-Field Method of Phase Transitions/Domain Structures in Ferroelectric Thin Films: A Review. *J. Am. Ceram. Soc.* **91,** 1835–1844. ISSN: 0002-7820, 1551-2916. http://doi.wiley.com/10.1111/j.1551-2916.2008.02413.x (2018) (June 2008).

70. Pertsev, N. A., Zembilgotov, A. G. & Tagantsev, A. K. Effect of Mechanical Boundary Conditions on Phase Diagrams of Epitaxial Ferroelectric Thin Films. *Phys. Rev. Lett.* **80,** 1988–1991. https://link.aps.org/doi/10.1103/PhysRevLett.80.1988 (2018) (Mar. 2, 1998).

71. Zhao, Z. *et al.* Grain-Size Effects on the Ferroelectric Behavior of Dense Nanocrystalline BaTiO3 Ceramics. *Phys. Rev. B* **70,** 024107. https://link.aps.org/doi/10.1103/PhysRevB.70.024107 (2018) (July 30, 2004).

72. Doersch, C. Tutorial on Variational Autoencoders. arXiv: 1606.05908 [cs, stat]. http://arxiv.org/abs/1606.05908 (2017) (June 19, 2016).

73. Radford, A., Metz, L. & Chintala, S. Unsupervised Representation Learning with Deep Convolutional Generative Adversarial Networks. arXiv: 1511.06434 [cs]. http://arxiv.org/abs/1511.06434 (2017) (Nov. 19, 2015).

74. Kingma, D. P. & Welling, M. Auto-Encoding Variational Bayes. arXiv: 1312.6114 [cs, stat]. http://arxiv.org/abs/1312.6114 (2018) (Dec. 20, 2013).

75. Ioffe, S. & Szegedy, C. Batch Normalization: Accelerating Deep Network Training by Reducing Internal Covariate Shift. arXiv: 1502.03167 [cs]. http://arxiv.org/abs/1502.03167 (2018) (Feb. 10, 2015).

76. Glorot, X. & Bengio, Y. *Understanding the Difficulty of Training Deep Feedforward Neural Networks* in *Proceedings of the Thirteenth International Conference on Artificial Intelligence and Statistics* (eds Teh, Y. W. & Titterington, M.) **9**

(PMLR, Chia Laguna Resort, Sardinia, Italy, May 13–15, 2010), 249–256. http://proceedings.mlr.press/v9/glorot10a.html.

77. Tieleman, T. & Hinton, G. Lecture 6.5—RmsProp: Divide the Gradient by a Running Average of Its Recent Magnitude (2012).

78. Xue, D. *et al.* Accelerated Search for Materials with Targeted Properties by Adaptive Design. *Nat Commun.* **7,** 11241. ISSN: 2041-1723. https://www.nature.com/articles/ncomms11241 (2018) (Apr. 15, 2016).

79. Ren, F. *et al.* Accelerated Discovery of Metallic Glasses through Iteration of Machine Learning and High-Throughput Experiments. *Sci. Adv.* **4,** eaaq1566. ISSN: 2375-2548. http://advances.sciencemag.org/content/4/4/eaaq1566 (2018) (Apr. 1, 2018).

80. Ward, L. & Wolverton, C. Atomistic Calculations and Materials Informatics: A Review. *Curr. Opin. Solid State Mater. Sci. Materials Informatics: Insights, Infrastructure, and Methods* **21,** 167–176. ISSN: 1359-0286. http://www.sciencedirect.com/science/article/pii/S1359028616301085 (2017) (June 1, 2017).

81. Kusne, A. G. *et al.* On-the-Fly Machine-Learning for High-Throughput Experiments: Search for Rare-Earth-Free Permanent Magnets. *Sci Rep.* **4.** ISSN: 2045-2322. pmid: 25220062. https://www.ncbi.nlm.nih.gov/pmc/articles/PMC4163667/ (2017) (Sept. 15, 2014).

82. Jain, A., Persson, K. A. & Ceder, G. Research Update: The Materials Genome Initiative: Data Sharing and the Impact of Collaborative Ab Initio Databases. *APL Mater.* **4,** 053102. http://aip.scitation.org/doi/abs/10.1063/1.4944683 (2017) (Mar. 24, 2016).

83. Holdren, J. P. *et al.* Materials Genome Initiative for Global Competitiveness. *National Science and technology council OSTP. Washington, USA* (2011).

84. McDowell, D. L. & Kalidindi, S. R. The Materials Innovation Ecosystem: A Key Enabler for the Materials Genome Initiative. *MRS Bulletin* **41,** 326–337. ISSN: 0883-7694, 1938-1425. https://www.cambridge.org/core/journals/mrs-bulletin/article/materials-innovation-ecosystem-a-key-enabler-for-the-materials-genome-initiative/179CF25E8B3101FBD6E81380F7364305 (2018) (Apr. 2016).

85. On Integrated Computational Materials Engineering, C. *Integrated Computational Materials Engineering: A Transformational Discipline for Improved Competitiveness and National Security* (National Academies Press, 2008).

86. V Balachandran, P., Theiler, J., Rondinelli, J. & Lookman, T. Materials Prediction via Classification Learning. *Sci Rep.* **5,** 13285 (Aug. 25, 2015).

87. Talapatra, A. *et al.* Towards an Autonomous Efficient Materials Discovery Framework: An Example of Optimal Experiment Design Under Model Uncertainty (Mar. 14, 2018).

88. Wang, J. *et al.* New Methods for Prediction of Elastic Constants Based on Density Functional Theory Combined with Machine Learning. *Computational Materials Science* **138,** 135–148 (Oct. 1, 2017).

89. Kumar, H., Briant, C. L. & Curtin, W. A. Using Microstructure Reconstruction to Model Mechanical Behavior in Complex Microstructures. *Mechanics of Materials. Advances in Disordered Materials* **38,** 818–832. ISSN: 0167-6636. http://www.sciencedirect.com/science/article/pii/S0167663605001638 (2018) (Aug. 1, 2006).

90. Torquato, S. *Random Heterogeneous Materials: Microstructure and Macroscopic Properties* 720 pp. ISBN: 978-1-4757-6355-3 (Springer Science & Business Media, Apr. 17, 2013).

91. Steinbach, I. Phase-Field Models in Materials Science. *Modelling Simul. Mater. Sci. Eng.* **17,** 073001. ISSN: 0965-0393. http://stacks.iop.org/0965-0393/17/i=7/a=073001 (2017) (2009).

92. Kalinin, S. V., Sumpter, B. G. & Archibald, R. K. BigDeepSmart Data in Imaging for Guiding Materials Design. *Nat Mater.* **14,** 973–980. ISSN: 1476-4660. https://www.nature.com/articles/nmat4395 (2018) (Oct. 2015).

93. DeCost, B. L., Jain, H., Rollett, A. D. & Holm, E. A. Computer Vision and Machine Learning for Autonomous Characterization of AM Powder Feedstocks. *JOM* **69,** 456–465. ISSN: 1047-4838, 1543-1851. https://link.springer.com/article/10.1007/s11837-016-2226-1 (2017) (Mar. 1, 2017).

94. Cang, R. & Ren, M. Y. Deep Network-Based Feature Extraction and Reconstruction of Complex Material Microstructures, V02BT03A008. http://dx.doi.org/10.1115/DETC2016-59404 (2018) (Aug. 21, 2016).

95. Huang, H., Yu, P. S. & Wang, C. An Introduction to Image Synthesis with Generative Adversarial Nets. arXiv: 1803.04469 [cs]. http://arxiv.org/abs/1803.04469 (2018) (Mar. 12, 2018).

96. Koukhar, V. G., Pertsev, N. A. & Waser, R. Thermodynamic Theory of Epitaxial Ferroelectric Thin Films with Dense Domain Structures. *Phys. Rev. B* **64,** 214103. https://link.aps.org/doi/10.1103/PhysRevB.64.214103 (2018) (Nov. 8, 2001).

97. Fousek, J. & Janovec, V. The Orientation of Domain Walls in Twinned Ferroelectric Crystals. *J. Appl. Phys.* **40,** 135–142. ISSN: 0021-8979. http://aip.scitation.org/doi/10.1063/1.1657018 (2018) (Jan. 1, 1969).

98. Randall, C. A., Kim, N., Kucera, J.-P., Cao, W. & Shrout, T. R. Intrinsic and Extrinsic Size Effects in Fine-Grained Morphotropic-Phase-Boundary Lead Zirconate Titanate Ceramics. *J. Am. Ceram. Soc.* **81,** 677–688. ISSN: 1551-2916. https:

//onlinelibrary.wiley.com/doi/abs/10.1111/j.1151-2916.1998.tb02389.x (2018) (Mar. 1, 1998).

99. Ivry, Y., Chu, D. P. & Durkan, C. Bundles of Polytwins as Meta-Elastic Domains in the Thin Polycrystalline Simple Multi-Ferroic System PZT. *Nanotechnology* **21,** 065702. ISSN: 0957-4484, 1361-6528. http://stacks.iop.org/0957-4484/21/i=6/a=065702?key=crossref.5f7fa26f8fe8441b1a4a877c5a5d4b61 (2019) (Feb. 10, 2010).

100. Ivry, Y., Scott, J. F., Salje, E. K. H. & Durkan, C. Nucleation, Growth, and Control of Ferroelectric-Ferroelastic Domains in Thin Polycrystalline Films. *Physical Review B* **86.** ISSN: 1098-0121, 1550-235X. https://link.aps.org/doi/10.1103/PhysRevB.86.205428 (2019) (Nov. 26, 2012).

101. Ivry, Y., Durkan, C., Chu, D. & Scott, J. F. Nano-Domain Pinning in Ferroelastic-Ferroelectrics by Extended Structural Defects. *Advanced Functional Materials* **24,** 5567–5574. ISSN: 1616301X. http://doi.wiley.com/10.1002/adfm.201304268 (2019) (Sept. 2014).

102. Marincel, D. M. *et al.* Domain Wall Motion Across Various Grain Boundaries in Ferroelectric Thin Films. *Journal of the American Ceramic Society* **98** (ed Damjanovic, D.) 1848–1857. ISSN: 00027820. http://doi.wiley.com/10.1111/jace.13535 (2019) (June 2015).

103. Majkut, M., Daniels, J. E., Wright, J. P., Schmidt, S. & Oddershede, J. Electromechanical Response of Polycrystalline Barium Titanate Resolved at the Grain Scale. *Journal of the American Ceramic Society* **100** (ed Ihlefeld, J.) 393–402. ISSN: 00027820. http://doi.wiley.com/10.1111/jace.14481 (2019) (Jan. 2017).

104. Brewer, S. *et al.* Piezoelectric Response Enhancement in the Proximity of Grain Boundaries of Relaxor-Ferroelectric Thin Films. *Applied Physics Letters* **108,** 242908.

ISSN: 0003-6951, 1077-3118. http://aip.scitation.org/doi/10.1063/1.4953575 (2019) (June 13, 2016).

105. Li, W., Field, K. G. & Morgan, D. Automated Defect Analysis in Electron Microscopic Images. *npj Computational Materials* **4,** 36. ISSN: 2057-3960. https://www.nature.com/articles/s41524-018-0093-8 (2018) (July 18, 2018).

106. DeCost, B. L., Francis, T. & Holm, E. A. High Throughput Quantitative Metallography for Complex Microstructures Using Deep Learning: A Case Study in Ultrahigh Carbon Steel. arXiv: 1805.08693 [cs]. http://arxiv.org/abs/1805.08693 (2018) (May 4, 2018).

107. Ronneberger, O., Fischer, P. & Brox, T. U-Net: Convolutional Networks for Biomedical Image Segmentation. arXiv: 1505.04597 [cs]. http://arxiv.org/abs/1505.04597 (2019) (May 18, 2015).

108. Vidyasagar, A., Tan, W. L. & Kochmann, D. M. Predicting the Effective Response of Bulk Polycrystalline Ferroelectric Ceramics via Improved Spectral Phase Field Methods. *Journal of the Mechanics and Physics of Solids* **106,** 133–151. ISSN: 0022-5096. http://www.sciencedirect.com/science/article/pii/S0022509617300595 (2018) (Sept. 1, 2017).

109. Shin, H. *et al.* Deep Convolutional Neural Networks for Computer-Aided Detection: CNN Architectures, Dataset Characteristics and Transfer Learning. *IEEE Transactions on Medical Imaging* **35,** 1285–1298. ISSN: 0278-0062 (May 2016).

110. Arjovsky, M., Chintala, S. & Bottou, L. Wasserstein GAN. arXiv: 1701.07875 [cs, stat]. http://arxiv.org/abs/1701.07875 (2019) (Jan. 26, 2017).

111. Wei, S.-E., Ramakrishna, V., Kanade, T. & Sheikh, Y. Convolutional Pose Machines. arXiv: 1602.00134 [cs]. http://arxiv.org/abs/1602.00134 (2019) (Jan. 30, 2016).

Appendix A: Supplemental Information

A.1 Characterizing Success

One of the more difficult challenges was determining how successful the model was a reproducing a statistically equivalent image. It is easy to see that the encoder-decoder in chapter 4 produces images that appear similar to the phase-field model outputs. However, there are a few important features that may provide an indication to how well the network is really learning. Some of the features that were worth observing were:

- Volume Fraction
- Grain boundary polarization
- Domain wall orientation
- Contiguity of domains
- Smoothness of domain walls
- Domain wall thickness
- Domain continuity across grain boundary

However, not all features are straightforward to quantify and have not been implemented. There may be many other features that are not preserved besides those listed here.

A.2 Hyper-parameter Tuning

A number of parameters were varied throughout the network process. As we decided on one network architecture, the number of filters for each the encoder and decoder and the size of the latent vector were varied. The results in Table A.1 demonstrates a few sample runs and how the results were changed by these updates.

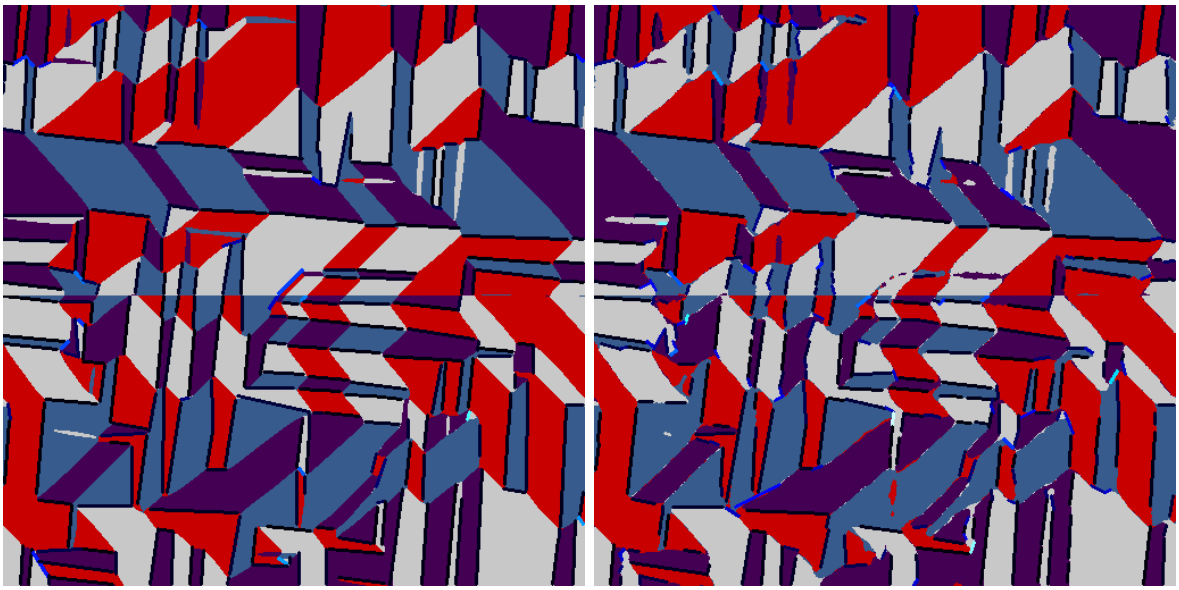

(a) phase-field **(b)** encoder-decoder

Figure A.1. Overlay with colored lines showing sources of error in detecting domain wall orientations. Blue and white lines indicate large dependency between detected orientation and expected orientation of that domain wall.

A.3 Application to Other Phase-Field Methods

While this work is limited in scope to evaluation of ferroelectric domains in $PbTiO_3$, there are many other potentially useful phase-field simulations that could be readily explored. First, one might be interested in how homogeneous and inhomogeneous stress affects precipitation in the microstructure over time. For example, consider the time evolution of a precipitate in a strained material, which can be seen in Figure A.2. It might be useful to consider and model the change in microstructure with time. This model could present a baseline which could be expanded for such applications.

A.4 Network Architecture

As previously mentioned there are two common types of network strategies that have been applied to MCR. The first is a Generative Adversarial Network (GAN) and the second is a Variational Auto-Encoder (VAE). A VAE operates by taking an input, compressing

Table A.1. A spread of different training runs performed with varying hyper-parameters. NEF is the number of filters used in the encoder as a starting point. NDF is likewise the number of filters used in the decoder.

Run	NEF	NDF	Nlatent	LR	Epochs	Avg Err	Med Err
1	16	16	512	1×10^{-5}	2320	1.4164	1.2291
2	16	16	512	1×10^{-5}	2840	1.3204	1.1631
3	16	16	512	1×10^{-5}	7300	1.2158	1.0605
4	8	8	16	1×10^{-4}	4500	2.0275	1.6463
5	8	8	16	1×10^{-5}	6960	1.8420	1.6181
6	8	8	64	1×10^{-5}	8000	1.6534	1.4840

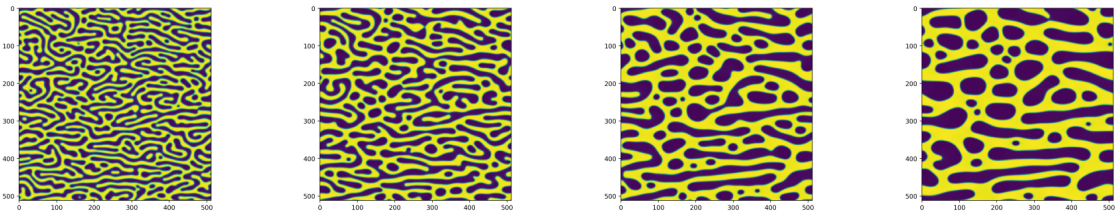

(a) $t = 40$ **(b)** $t = 120$ **(c)** $t = 400$ **(d)** $t = 1000$

Figure A.2. Precipitation over time in inhomogeneous material.

it down to a latent vector, and then attempting to regenerate the input. This is very straightforward to train, as the loss function is a straightforward L2 loss of the input compared with the output. VAEs provide a compressed latent representation, which can be useful to perform imputation or other model tweaks. However, VAEs can often produce blurry results, especially when used in the vanilla Gaussian reconstruction model.

GANs operate on a different basis and instead use adversarial networks. They use a discriminator, an external network trained to distinguish the true image from the fake image. The goal is to take some input sample and use that to generate an example that is realistic enough to fool the discriminator. Training is often quite complicated as the loss function is a highly complex network. It is common for GANs to suffer from mode collapse, where there is little variance in the output of the generator. See Figure A.3 and Figure A.4 for examples of mode collapse. One method for circumventing mode collapse is to use the Wasserstein GAN [110]. GANs often produce much higher visual fidelity.

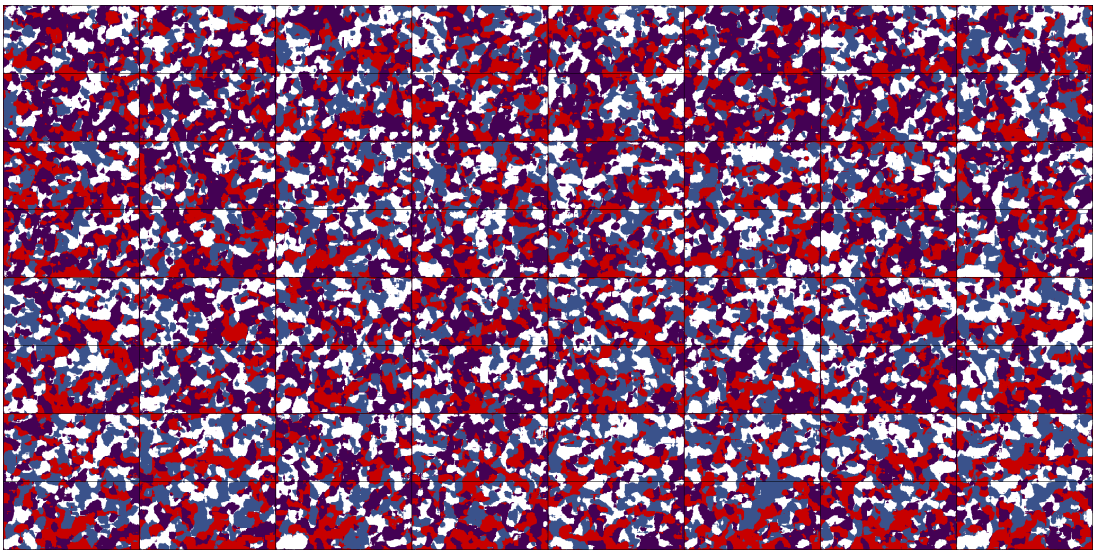

Figure A.3. Output of GAN with 2000 training data on bi-crystals demonstrating mode collapse.

A.5 Effective Receptive Field

One important aspect of this work is the ability of neural networks to capture long-range interactions. Something on one side of the microstructure can interact with something on another. The range of interactions that can be observed is called the effective receptive field (ERF). There is basic theory on how that can be determined [111]. In principle, the effect of each pixel in the ERF does not contribute equally to the final product. There are many ways to increase the effective receptive field. Stacking more layers (increasing depth), subsampling (pooling, striding), filter dilation (dilated convolutions), etc.

Figure A.5 captures the premise of how the receptive field increases with a deeper network topology and more pooling layers. After just a single 9×9 convolutional layer, the receptive field is only 9 pixels long on a side. By applying pooling and another convolution, the network now interconnects more pixels and is able to generalize a larger area. The effective receptive field is now 26 pixels wide on a side.

Although the effective receptive field should be considered at least as large as the smallest interaction being considered, it might be productive to study the effect of the

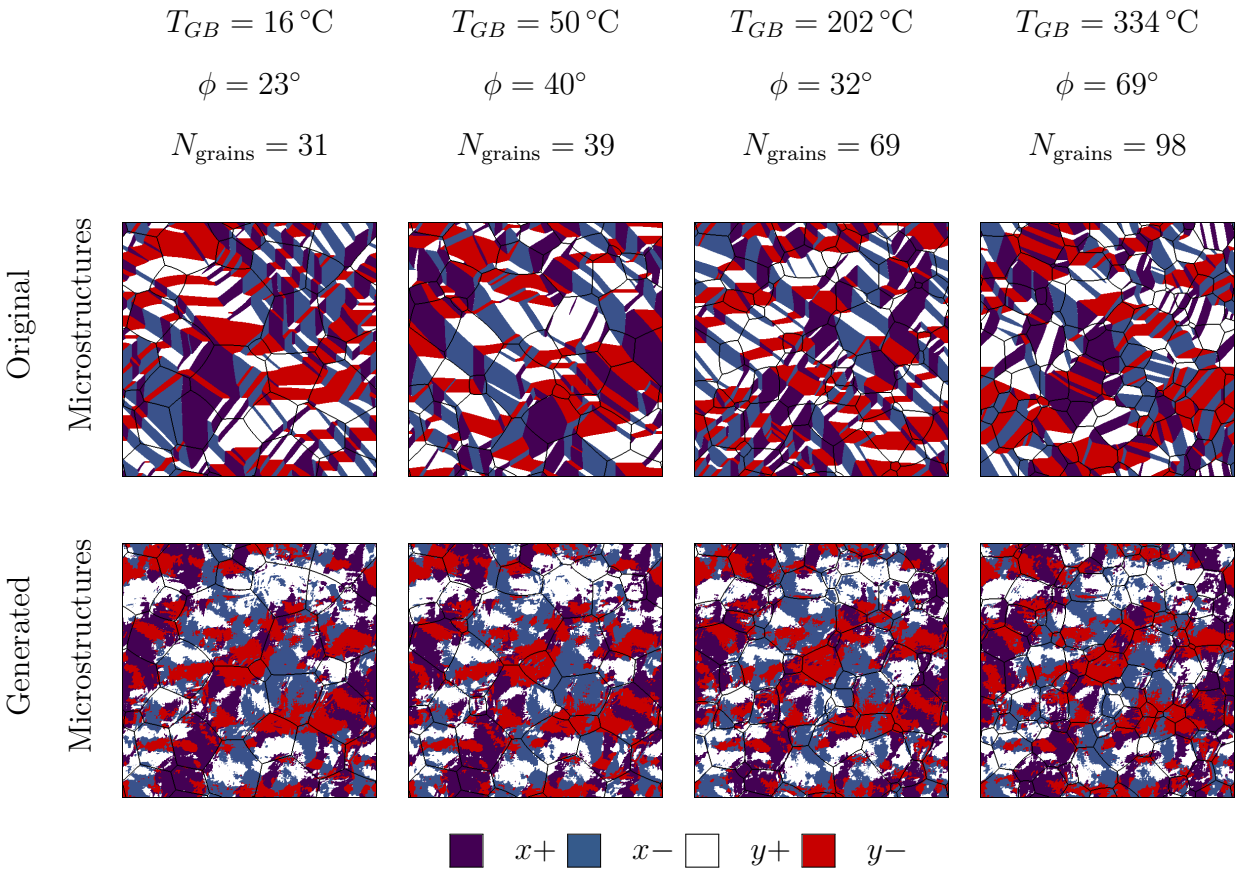

Figure A.4. Another example of GAN mode collapse with a supplemental L2 loss function.

receptive field. Does observing only small features still provide good results? Are the large interactions or features necessary for the property you are looking at? It may be worth considering different receptive fields to understand more about the problem you are studying.

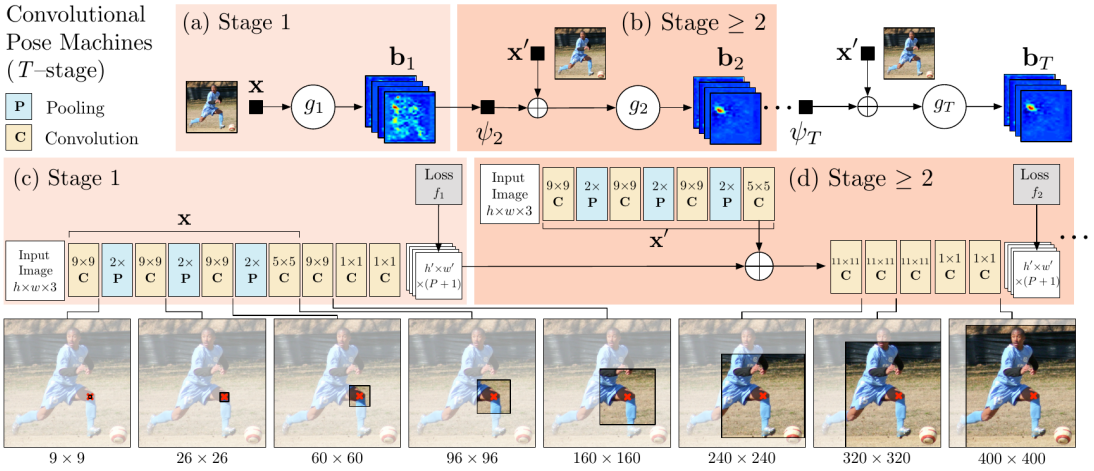

Figure A.5. The effective receptive fields from Wei et al [111]. This demonstrates how the effective field grows with larger kernel sizes and decreasing image size through a multilayer convolutional network.

A.6 Image to Image Method

A variational autoencoder typically uses a direct loss between the input and generated output. However, in our case, we use a network framework similar to a variational autoencoder but we encode a set of input parameters. This is not ideal. It is difficult to map input parameters to microstructure directly because it is a one-to-many operation. There are an infinite number of microstructures that may result from the same set of input conditions. Image-to-Image gives us a baseline of how well we can do with L2 loss, since this is the ideal case of building an image mapping. The encoder is not dealing with overlapping input parameters and multiple outputs for similar inputs. Instead, it is given an image and attempts to compress and reproduce that image.